The Impact of Anisotropic Covariance Structure on the Training Dynamics and Generalization Error of Linear Networks

Anonymous authors
Paper under double-blind review

Abstract

The success of deep neural networks largely depends on the statistical structure of the training data. While learning dynamics and generalization on isotropic data are well-established, the impact of pronounced anisotropy on these crucial aspects is not yet fully understood. We examine the impact of data anisotropy, represented by a spiked covariance structure, a canonical yet tractable model, on the learning dynamics and generalization error of a two-layer linear network in a linear regression setting. Our analysis reveals that the learning dynamics proceed in two distinct phases, governed initially by the input-output correlation and subsequently by other principal directions of the data structure. Furthermore, we derive an analytical expression for the generalization error, quantifying how the alignment of the spike structure of the data with the learning task improves performance. Our findings offer deep theoretical insights into how data anisotropy shapes the learning trajectory and final performance, providing a foundation for understanding complex interactions in more advanced network architectures.

1 Introduction

Deep learning has achieved remarkable success in diverse fields, ranging from image recognition to natural language processing, over the past decade. A key factor contributing to the high performance of deep learning is the availability of vast amounts of training data. While deep networks perform well at learning complex patterns from large data volumes, their performance is inherently sensitive to the underlying statistical structure of the data. Therefore, understanding how the data structure influences learning dynamics and generalization performance remains a fundamental problem in deep learning research.

The inherent non-linearity of deep networks makes a theoretical analysis of their learning process difficult. Consequently, simplified models, such as linear networks, are often employed. Although linear networks are less expressive than non-linear networks, they provide a tractable framework for analyzing important aspects of deep learning, including convergence (Arora et al., 2018; Du & Hu, 2019), learning dynamics (Saxe et al., 2013; 2019; Arora et al., 2018; Tarmoun et al., 2021; Min et al., 2021; Atanasov et al., 2022; Braun et al., 2022; Dominé et al., 2024; Kunin et al., 2024), and implicit bias of gradient descent (Arora et al., 2019; Woodworth et al., 2020; Pesme et al., 2021; Kunin et al., 2023; Varre et al., 2023).

The learning dynamics of linear networks are well-understood when the input data is isotropic. Under this condition, we can derive exact expressions for learning trajectories under certain initial conditions. However, real-world data is rarely isotropic, as many datasets exhibit complex anisotropic structures, where the variance is heterogeneously distributed, often being predominantly captured by a subset of principal components. Extending these theories to anisotropic data settings is notably challenging, even for these simple linear models (Tarmoun et al., 2021). Thus, a deeper theoretical understanding of how data anisotropy shapes learning trajectories and affects generalization performance is crucial.

In this study, we investigate the impact of data anisotropy on the learning dynamics and generalization performance of linear networks. We consider a linear regression problem where the input data is generated from a spiked covariance model. This model introduces controlled anisotropy by featuring one large eigenvalue (the spike) and small remaining eigenvalues. Specifically, we examine how spike magnitude and spike-target alignment affect the learning dynamics and generalization.

Our approach yields several important results. First, we identify distinct learning phases determined by the anisotropic data structure. To analyze the weight dynamics in the learning phases, we introduce a basis that captures the anisotropic structure of the input data. By effectively reducing the dimensionality of the dynamics, this framework allows us to simplify the description of the dynamics and consistently explain the overall weight evolution. Second, we derive an analytical expression for the generalization error of linear models trained on spiked covariance data. These findings provide a deeper theoretical understanding of learning under anisotropic data, establishing a crucial perspective for analyzing the behavior of more complex neural network architectures.

Our contributions are as follows:

- We demonstrate that two-layer linear networks trained on spiked covariance data exhibit distinct two-phase learning dynamics. We show that data anisotropy is essential for the existence of the later phase, as in its absence the dynamics reduce to the behavior in isotropic settings analyzed in previous studies (Section 3).
- We develop an analytical framework that reduces the high-dimensional dynamics to a tractable two-variable system of differential equations. This approach clearly identifies the mechanisms governing weight evolution and the existence of the two learning phases (Section 3.2).
- We derive an analytical expression for the generalization error, explicitly quantifying its dependence on data anisotropy, namely the magnitude and alignment of the spike with the target vector (Section 4).

1.1 Related Work

While a linear network is representationally equivalent to a single-layer model, its multi-layer structure introduces non-linear learning dynamics. Consequently, linear networks have been widely used to understand the learning dynamics of deep neural networks. Numerous important insights have been obtained for linear networks, including their loss landscape (Baldi & Hornik, 1989; Fukumizu, 1998), convergence properties (Arora et al., 2018; Du & Hu, 2019), generalization capabilities (Lampinen & Ganguli, 2018; Poggio et al., 2018; Advani et al., 2020; Huh, 2020; Gunasekar et al., 2018), and the implicit bias of gradient descent (Arora et al., 2019; Woodworth et al., 2020; Pesme et al., 2021; Kunin et al., 2023; Varre et al., 2023).

The analytical tractability of linear network dynamics is significantly enhanced when the input data is whitened. Under this assumption, exact solutions for the learning dynamics have been derived in several cases (Fukumizu, 1998; Saxe et al., 2013; 2019; Arora et al., 2018; Tarmoun et al., 2021; Min et al., 2021; Atanasov et al., 2022; Braun et al., 2022; Dominé et al., 2024; Kunin et al., 2024). For instance, Saxe et al. (2013; 2019) demonstrated that for deep linear networks with small or specific spectral initialization, the learning process decouples into independent modes governed by the singular values of the weight matrices. In another analysis with specific balanced initialization, the dynamics can be described by matrix Riccati equations, which have closed-form solutions (Fukumizu, 1998; Braun et al., 2022; Tarmoun et al., 2021; Dominé et al., 2024).

In anisotropic settings, the symmetries that simplify analysis in the isotropic case, such as the rotational invariance of the input data distribution, are absent. This absence generally makes the derivation of exact closed-form solutions for weight evolution intractable, even for linear networks. For example, Tarmoun et al. (2021) suggest that obtaining exact dynamics for general anisotropic data is broadly unachievable. Consequently, research often turns to alternative approaches, such as perturbation analysis (Gidel et al., 2019) and fixed-point analysis (Zhang et al., 2024).

To describe the learning dynamics of linear networks under general data in more detail, Advani et al. (2020) provided a set of dynamical equations for multi-layer linear networks under small initialization, linking their behavior to that of linear networks in which the weight matrix has a rank-one structure. While this observation has been used to analyze various phenomena in linear networks (Shan & Bordelon, 2021; Ji & Telgarsky, 2018; Marion & Chizat, 2024) , their contribution centered on deriving these reduced equations rather than providing explicit solutions for general anisotropic data. More recently, Atanasov et al. (2022) identified two-phase learning dynamics in linear networks under small initialization . They provide exact solutions for isotropic data, but their analytical approach for anisotropic data relies on an initial linearization approximation. Consequently, while identifying the early-phase alignment with the input-output correlation direction , they cannot capture its subsequent nonlinear weight saturation. For the later phase, they deduce that weights must realign to converge, but leave its nonlinear trajectory analytically unresolved. Our work directly addresses these limitations by using a spiked covariance model to reduce the high-dimensional dynamics into a tractable two-variable system. This allows us to characterize the mechanisms and derive explicit timescales for both early-phase saturation and later-phase realignment.

Beyond training dynamics, understanding the generalization performance of neural networks, especially in overparameterized regimes, is a crucial challenge. Gradient-based optimization in such models often exhibits an implicit bias towards solutions with specific properties, such as minimum-norm solutions in linear models with small initialization (Gunasekar et al., 2017; 2018; Arora et al., 2019; Min et al., 2021; Yun et al., 2021). The generalization error of these solutions, particularly in high-dimensional settings, has been intensely studied, with random matrix theory proving to be a powerful tool for precise characterization (Bartlett et al., 2020; Belkin et al., 2020; Mei & Montanari, 2022; Atanasov et al., 2024). Random matrix theory has yielded key insights, enabling exact calculations of generalization error for models like ridgeless and kernel regression, and elucidating dependencies on dimensionality, sample size, and noise, including the "double descent" phenomenon (Adlam & Pennington, 2020; Hastie et al., 2022; Canatar et al., 2021). These advancements allow for a more detailed understanding of how data anisotropies influence generalization (Wu & Xu, 2020; Richards et al., 2021; Mel & Ganguli, 2021; Mel & Pennington, 2021; Wei et al., 2022). While some studies examine the generalization error dynamics (e.g., Pezeshki et al. (2022)), they typically assume only one layer is optimized. In contrast, we analyze the final generalization error for two-layer linear networks with joint updates. By applying the theoretical foundations of random matrix theory, our work provides a precise analytical expression for the spiked covariance model that explicitly quantifies the error's dependence on two key aspects of the anisotropy, namely, the spike's magnitude and its alignment with the target vector.

2 Preliminaries

In this study, we investigate a standard high-dimensional linear regression problem with structured data, using linear networks trained via gradient descent.

2.1 Generative model

We consider a dataset of n input-output pairs $\{(\boldsymbol{x}_i, y_i)\}_{i=1}^n$, where $\boldsymbol{x}_i \in \mathbb{R}^d$ and $y_i \in \mathbb{R}$. The input data $\boldsymbol{x}_i$ is drawn from a multivariate Gaussian distribution with zero mean and a covariance matrix $\boldsymbol{\Sigma} \in \mathbb{R}^{d\times d}$ given by

$$\boldsymbol{\Sigma} = \sigma^2(\boldsymbol{I} + \rho\boldsymbol{\mu}\boldsymbol{\mu}^\top), \tag{1}$$

where $\|\boldsymbol{\mu}\| = 1$. The covariance matrix $\boldsymbol{\Sigma}$ has one eigenvalue $\sigma^2(1+\rho)$ corresponding to the eigenvector $\boldsymbol{\mu}$ (the spike direction), and $d-1$ eigenvalues equal to σ^2 in the subspace orthogonal to $\boldsymbol{\mu}$. This model is known as the spiked covariance model (Johnstone, 2001). The output $y_i \in \mathbb{R}$ is given by

$$y_i = \boldsymbol{\beta}^\top \boldsymbol{x}_i, \tag{2}$$

where $\boldsymbol{\beta} \in \mathbb{R}^d$ is the target vector with $\|\boldsymbol{\beta}\| = 1$. We define the spike-target alignment as $A = \boldsymbol{\mu}^\top\boldsymbol{\beta}$. Without loss of generality, we can assume $A \geq 0$, as the sign of $\boldsymbol{\mu}$ can be flipped without changing the covariance matrix $\boldsymbol{\Sigma}$. Using this target vector, the input-output correlation is given by

$$\boldsymbol{\Sigma}_{xy} = \mathbb{E}[y\boldsymbol{x}] = \boldsymbol{\Sigma}\boldsymbol{\beta}. \tag{3}$$

In this paper, we investigate how the dynamics and generalization error of a linear network depend on the spike magnitude ρ and the spike-target alignment A.

2.2 Two-layer linear network

A two-layer linear network of width m is defined as

$$f(\boldsymbol{x}) = \boldsymbol{a}^\top \boldsymbol{W}\boldsymbol{x}. \tag{4}$$

Here $\boldsymbol{x} \in \mathbb{R}^d$ is the input, $\boldsymbol{W} \in \mathbb{R}^{m\times d}$ and $\boldsymbol{a} \in \mathbb{R}^m$ are the weight parameters for the first and second layers, respectively. In particular, we consider the case where $m \geq d$.

For analytical tractability, the network is initialized with small random weights whose variances are scaled by s^2 (where $s \ll 1$ is the initialization scale), and is trained using full-batch gradient descent with learning rate η (or time constant $\tau = 1/2\eta$) to minimize the squared error on the training dataset:

$$\mathcal{L}(\boldsymbol{W}, \boldsymbol{a}) = \frac{1}{n}\sum_{i=1}^{n}\left(f(\boldsymbol{x}_i) - y_i\right)^2. \tag{5}$$

In the limit of an infinitesimal learning rate, the learning dynamics of gradient descent are well approximated by the following gradient flow:

$$\tau\frac{d}{dt}\boldsymbol{W} = \boldsymbol{a}\left(\hat{\boldsymbol{\Sigma}}_{xy}^\top - \boldsymbol{a}^\top\boldsymbol{W}\hat{\boldsymbol{\Sigma}}\right), \tag{6}$$

$$\tau\frac{d}{dt}\boldsymbol{a}^\top = \left(\hat{\boldsymbol{\Sigma}}_{xy}^\top - \boldsymbol{a}^\top\boldsymbol{W}\hat{\boldsymbol{\Sigma}}\right)\boldsymbol{W}^\top, \tag{7}$$

where $\hat{\boldsymbol{\Sigma}}_{xy}$ denotes the empirical input-output correlation, and $\hat{\boldsymbol{\Sigma}}$ denotes the empirical input covariance:

$$\hat{\boldsymbol{\Sigma}}_{xy} = \frac{1}{n}\sum_{i=1}^{n} y_i\boldsymbol{x}_i, \quad \hat{\boldsymbol{\Sigma}} = \frac{1}{n}\sum_{i=1}^{n}\boldsymbol{x}_i\boldsymbol{x}_i^\top. \tag{8}$$

3 Learning Dynamics in Two-Layer Linear Network under Spiked Covariance Model

3.1 Empirical Observations

We begin by empirically examining the learning dynamics of a two-layer linear network using numerical simulations. To capture the essential behavior of the weight parameters, we show the learning trajectory in a two-dimensional phase plane defined by the coordinates $\hat{\boldsymbol{r}}_1^\top\boldsymbol{W}\boldsymbol{\mu}$ and $\hat{\boldsymbol{r}}_1^\top\boldsymbol{W}\boldsymbol{\mu}_\perp$, where $\hat{\boldsymbol{r}}_1$ is a fixed vector and $\boldsymbol{\mu}_\perp$ denotes a vector orthogonal to $\boldsymbol{\mu}$. Figure 1 shows this trajectory, together with orthogonal lines whose directions are defined by the vectors $\boldsymbol{v}_1$ and $\boldsymbol{v}_2$ (precise definitions of $\hat{\boldsymbol{r}}_1$, $\boldsymbol{v}_1$, and $\boldsymbol{v}_2$ are provided in the subsequent subsection). The learning trajectory clearly exhibits two distinct phases. It initially evolves primarily along the direction of $\boldsymbol{v}_1$, then makes a sharp turn and develops along $\boldsymbol{v}_2$ until it converges to the final solution.

These two-phase learning dynamics are also evident in the time evolution of the training loss. In Figure 2, we plot the loss together with the temporal evolution of the $\boldsymbol{v}_1$ and $\boldsymbol{v}_2$ components of $\hat{\boldsymbol{r}}_1^\top\boldsymbol{W}$, namely, $\hat{\boldsymbol{r}}_1^\top\boldsymbol{W}\boldsymbol{v}_1$ and $\hat{\boldsymbol{r}}_1^\top\boldsymbol{W}\boldsymbol{v}_2$. Initially, the training loss remains on a plateau before dropping sharply. This drop corresponds to the rapid growth of the $\boldsymbol{v}_1$ component of $\hat{\boldsymbol{r}}_1^\top\boldsymbol{W}$, while the $\boldsymbol{v}_2$ component remains negligible. Subsequently, the loss decreases smoothly, driven by the growth of the $\boldsymbol{v}_2$ component of $\hat{\boldsymbol{r}}_1^\top\boldsymbol{W}$ and adjustments to the $\boldsymbol{v}_1$ component.

Based on these empirical observations, we define two distinct phases of learning: an *early phase*, characterized by the rapid growth of the $\boldsymbol{v}_1$ component of $\hat{\boldsymbol{r}}_1^\top\boldsymbol{W}$, and a *later phase*, characterized by the subsequent growth of its $\boldsymbol{v}_2$ component. In the following, we provide a theoretical analysis of these observed dynamics.

3.2 Theoretical Analysis

To analyze the two-phase behavior, we consider the limit as $n \to \infty$ with fixed input dimension d, such that the empirical covariance matrices $\hat{\boldsymbol{\Sigma}}$ and the empirical input-output correlation vector $\hat{\boldsymbol{\Sigma}}_{xy}$ converge to their population counterparts, $\hat{\boldsymbol{\Sigma}} \to \boldsymbol{\Sigma}$ and $\hat{\boldsymbol{\Sigma}}_{xy} \to \boldsymbol{\Sigma}_{xy} = \boldsymbol{\Sigma}\boldsymbol{\beta}$, respectively.

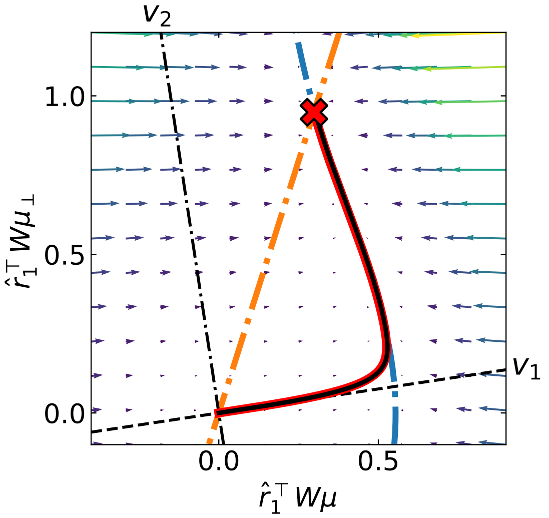

Figure 1: Learning trajectories in a phase plane with the spike direction $\boldsymbol{\mu}$ as the horizontal axis and the perpendicular direction $\boldsymbol{\mu}_\perp = (\boldsymbol{I} - \boldsymbol{\mu}\boldsymbol{\mu}^\top)\boldsymbol{\beta}/\|(\boldsymbol{I} - \boldsymbol{\mu}\boldsymbol{\mu}^\top)\boldsymbol{\beta}\|$ as the vertical axis. The vector field and nullclines (blue: $dw_1/dt = 0$, orange: $dw_2/dt = 0$) are from the reduced two-variable dynamics (Equations (16) and (17)). The red trajectory is projected from a simulation, while the black trajectory is from the reduced two-variable dynamics (Equations (16) and (17)). The basis directions, $\boldsymbol{v}_1$ (dashed) and $\boldsymbol{v}_2$ (dash-dotted), are also shown. The close match between trajectories validates the dimensionality reduction analysis. The parameters are set to $A = 0.3$, $\rho = 20$, and $\sigma^2 = 1$, with the number of training samples $n = 10000$. The network parameters are $d = 30$ and $m = 50$ and the initialization is performed as $W_{ij} \sim \mathcal{N}(0, s^2/d)$ and $a_i \sim \mathcal{N}(0, s^2/m)$ with $s = 10^{-5}$.

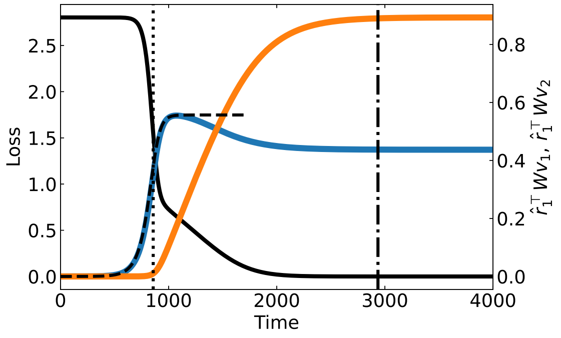

Figure 2: Time evolution of the training loss and magnitudes of weight components. The plotted values are the numerically obtained training loss (black) and the projections of the weight vectors $\boldsymbol{w}_1$ (blue) and $\boldsymbol{w}_2$ (orange) onto the initial growth direction $\hat{\boldsymbol{r}}_1$, namely, $\hat{\boldsymbol{r}}_1^\top \boldsymbol{W}\boldsymbol{v}_1$ and $\hat{\boldsymbol{r}}_1^\top \boldsymbol{W}\boldsymbol{v}_2$, respectively. The black dashed line is the analytical approximation for the early phase given by Equation (22) , with its initial value determined by Equation (18). Vertical dotted lines and vertical dash-dotted lines indicate characteristic timescales for the early and later phases, respectively, with the latter defined in Inequality (23) using $\delta = 3$. The parameters are the same as those in Figure 1.

3.2.1 Dimensionality Reduction to a Two-Variable System

To reduce the dimensionality of the dynamics, we first introduce a basis adapted to the data structure, designed to capture the principal axes of learning and thus allowing for a clear characterization of each phase. We construct this basis, denoted by the matrix $\boldsymbol{V} = (\boldsymbol{v}_1, \boldsymbol{v}_2, \ldots, \boldsymbol{v}_d) \in \mathbb{R}^{d\times d}$, as follows:

- The first basis vector is defined as $\boldsymbol{v}_1 = \boldsymbol{\Sigma}_{xy}/\|\boldsymbol{\Sigma}_{xy}\|$, to capture the weight growth along the input-output correlation direction in the early phase.
- The second basis vector, $\boldsymbol{v}_2$, is defined based on the alignment of $\boldsymbol{\Sigma}_{xy}$ and $\boldsymbol{\beta}$. If they are not parallel, $\boldsymbol{v}_2$ is defined as the normalized vector in the plane spanned by $\{\boldsymbol{\Sigma}_{xy}, \boldsymbol{\beta}\}$ that is orthogonal to $\boldsymbol{v}_1$. In this case, it captures the adjustment of the weights toward $\boldsymbol{\beta}$. The sign of $\boldsymbol{v}_2$ will be specified just below for analytical convenience. In the parallel case, where no such adjustment occurs, $\boldsymbol{v}_2$ is simply chosen as any normalized vector orthogonal to $\boldsymbol{v}_1$ to complete the basis.
- The remaining vectors, $\{\boldsymbol{v}_3, \ldots, \boldsymbol{v}_d\}$, form an orthonormal basis for the subspace orthogonal to the span of $\{\boldsymbol{\Sigma}_{xy}, \boldsymbol{\beta}\}$.

Using the basis $\boldsymbol{V}$, we can represent the weight matrix as $\boldsymbol{W} = (\boldsymbol{w}_1, \boldsymbol{w}_2, \ldots, \boldsymbol{w}_d)\boldsymbol{V}^\top$. By substituting this expression into the gradient flow equation (Equation (6)), we obtain the following dynamics for each component vector:

$$\tau \frac{d}{dt}\boldsymbol{w}_1 = \|\boldsymbol{\Sigma}_{xy}\|\boldsymbol{a} - (\lambda_1 \boldsymbol{a}^\top \boldsymbol{w}_1 - \nu \boldsymbol{a}^\top \boldsymbol{w}_2)\boldsymbol{a}, \tag{9}$$

$$\tau \frac{d}{dt}\boldsymbol{w}_2 = -(-\nu \boldsymbol{a}^\top \boldsymbol{w}_1 + \lambda_2 \boldsymbol{a}^\top \boldsymbol{w}_2)\boldsymbol{a}, \tag{10}$$

$$\tau \frac{d}{dt}\boldsymbol{w}_i = -\sigma^2 \boldsymbol{a}^\top \boldsymbol{w}_i \boldsymbol{a}, \quad (i = 3, \ldots, d). \tag{11}$$

Similarly, from Equation (7), the dynamics for the second-layer weight $\boldsymbol{a}$ are given by:

$$\tau \frac{d}{dt}\boldsymbol{a} = \|\boldsymbol{\Sigma}_{xy}\|\boldsymbol{w}_1 - (\lambda_1 \boldsymbol{a}^\top \boldsymbol{w}_1 - \nu \boldsymbol{a}^\top \boldsymbol{w}_2)\boldsymbol{w}_1 - (-\nu \boldsymbol{a}^\top \boldsymbol{w}_1 + \lambda_2 \boldsymbol{a}^\top \boldsymbol{w}_2)\boldsymbol{w}_2 - \sum_{i=3}^{d} \sigma^2 \boldsymbol{a}^\top \boldsymbol{w}_i \boldsymbol{w}_i, \tag{12}$$

where $\lambda_1 = \boldsymbol{v}_1^\top \boldsymbol{\Sigma} \boldsymbol{v}_1$, $\lambda_2 = \boldsymbol{v}_2^\top \boldsymbol{\Sigma} \boldsymbol{v}_2$, and $\nu = -\boldsymbol{v}_1^\top \boldsymbol{\Sigma} \boldsymbol{v}_2$. Here, we choose the direction of $\boldsymbol{v}_2$ so that ν is positive. The derivation of Equations (9) to (12), together with explicit forms of $\|\boldsymbol{\Sigma}_{xy}\|$, λ_1, λ_2, and ν , is given in Appendix A.

With the dynamics expressed in this adapted basis, we can further reduce the high-dimensional system by isolating the active subspace. From Equation (11), it follows that $\tau \frac{d}{dt}\|\boldsymbol{w}_i\|^2 = -2\sigma^2(a^\top w_i)^2 \leq 0$ for $i \geq 3$. This guarantees that the magnitude of these components is monotonically non-increasing. Since the initial values $\boldsymbol{w}_i(0)$ are of scale $O(s)$, these components remain bounded by $O(s)$ throughout the entire training. Thus, the overall dynamics are effectively confined to the subspace spanned by $\boldsymbol{w}_1$, $\boldsymbol{w}_2$, and $\boldsymbol{a}$.

Focusing on this restricted subspace, we can now examine the beginning of learning. For a two-layer linear network initialized at the small scale s, its dynamics can be approximated by linear differential equations by neglecting higher-order terms:

$$\tau \frac{d}{dt}\boldsymbol{w}_1 = \|\boldsymbol{\Sigma}_{xy}\|\boldsymbol{a} + O(s^3), \quad \tau \frac{d}{dt}\boldsymbol{a} = \|\boldsymbol{\Sigma}_{xy}\|\boldsymbol{w}_1 + O(s^3) \tag{13}$$

while $\tau d\boldsymbol{w}_2/dt = O(s^3)$. These equations decouple into an exponentially growing mode $(\boldsymbol{a} + \boldsymbol{w}_1)/2$ and a decaying mode $(\boldsymbol{a} - \boldsymbol{w}_1)/2$. Consequently, $\boldsymbol{w}_1$ and $\boldsymbol{a}$ rapidly align and grow symmetrically along the input-output correlation direction $\boldsymbol{v}_1 = \boldsymbol{\Sigma}_{xy}/\|\boldsymbol{\Sigma}_{xy}\|$. In contrast, $\boldsymbol{w}_2$ lacks this initial driving force and remains at the initialization scale $O(s)$. The following lemma formalizes the exponential growth of these dominant components, $\boldsymbol{w}_1$ and $\boldsymbol{a}$, at the beginning of learning:

Lemma 3.1. *There exists a constant $C > 0$ such that for all sufficiently small $s > 0$ and for all $0 \leq t < \frac{2\tau}{3(\|\boldsymbol{\Sigma}_{xy}\| + 2\operatorname{Tr}\boldsymbol{\Sigma})} \log \frac{1}{s}$, the solutions $\boldsymbol{w}_1$ and $\boldsymbol{a}$ to Equation (13) satisfy*

$$\left\|\boldsymbol{w}_1(t) - \boldsymbol{r}_1 e^{\|\boldsymbol{\Sigma}_{xy}\|t/\tau}\right\| \leq Cs, \quad \left\|\boldsymbol{a}(t) - \boldsymbol{r}_1 e^{\|\boldsymbol{\Sigma}_{xy}\|t/\tau}\right\| \leq Cs \tag{14}$$

where $\boldsymbol{r}_1 = (\boldsymbol{a}(0) + \boldsymbol{w}_1(0))/2$.

The proof of Lemma 3.1 is in Appendix B.1. This result indicates that the weights initially grow along the direction $\hat{\boldsymbol{r}}_1 = \boldsymbol{r}_1/\|\boldsymbol{r}_1\|$. The following lemma establishes that these vectors remain confined to this initial growth direction throughout the entire learning phase, with the orthogonal components strictly bounded by $O(s)$:

Lemma 3.2. *Let $\boldsymbol{P}_\perp = \boldsymbol{I} - \hat{\boldsymbol{r}}_1 \hat{\boldsymbol{r}}_1^\top$ be the projection operator. There exists a constant $C_\perp > 0$ such that for all sufficiently small $s > 0$ and for all $t \geq 0$, the orthogonal components of the trajectories satisfy:*

$$\|\boldsymbol{P}_\perp \boldsymbol{a}(t)\| + \|\boldsymbol{P}_\perp \boldsymbol{w}_1(t)\| + \|\boldsymbol{P}_\perp \boldsymbol{w}_2(t)\| \leq C_\perp s. \tag{15}$$

The proof of Lemma 3.2 is deferred to Appendix B.3.

This rank-one condensation enables us to describe the evolution of these vectors using only their scalar magnitudes: $\boldsymbol{a}(t) \approx a(t)\hat{\boldsymbol{r}}_1$, $\boldsymbol{w}_1(t) \approx w_1(t)\hat{\boldsymbol{r}}_1$, and $\boldsymbol{w}_2(t) \approx w_2(t)\hat{\boldsymbol{r}}_1$. This effectively reduces the dimensionality of the problem and implies that the first-layer weight matrix can be approximated as $\boldsymbol{W} \approx \hat{\boldsymbol{r}}_1\boldsymbol{w}(t)^\top\boldsymbol{V}^\top$, where $\boldsymbol{w}(t) = (w_1(t), w_2(t), 0, \dots, 0)^\top$. This rank-one structure of the weight matrix is consistent with findings in previous research (Advani et al., 2020; Atanasov et al., 2022; Shan & Bordelon, 2021; Ji & Telgarsky, 2018; Marion & Chizat, 2024) .

To further decouple the system, we employ a conservation law $\frac{d}{dt}(\boldsymbol{a}\boldsymbol{a}^\top - \sum_{i=1}^d \boldsymbol{w}_i\boldsymbol{w}_i^\top) = 0$, which can be derived from the fact that the time derivatives of $\boldsymbol{a}\boldsymbol{a}^\top$ and $\boldsymbol{W}\boldsymbol{W}^\top$ are identical under the gradient flow dynamics (Equations (6) and (7)). Considering the initialization condition, this implies $\boldsymbol{a}\boldsymbol{a}^\top - \sum_{i=1}^d \boldsymbol{w}_i\boldsymbol{w}_i^\top = O(s^2)$ for all time. Given that $\boldsymbol{w}_i$ for $i \geq 3$ remain at $O(s)$, taking the trace simplifies this relation to $a(t)^2 \approx w_1(t)^2 + w_2(t)^2$. This allows us to eliminate $a(t)$ and exactly reduce the high-dimensional dynamics into a closed two-variable system, formally established in the following theorem:

Theorem 3.3. *Suppose the original two-layer linear network is initialized at a sufficiently small scale $s > 0$. Let (w_1, w_2) be the unique solution to the initial value problem*

$$\tau\frac{d}{dt}w_1 = \|\boldsymbol{\Sigma}_{xy}\|\sqrt{w_1^2 + w_2^2} - \lambda_1 w_1(w_1^2 + w_2^2) + \nu w_2(w_1^2 + w_2^2), \tag{16}$$

$$\tau\frac{d}{dt}w_2 = \nu w_1(w_1^2 + w_2^2) - \lambda_2 w_2(w_1^2 + w_2^2), \tag{17}$$

with initial conditions defined by the projections of the network's initial weights

$$w_1(0) = \frac{1}{2}\left[\hat{\boldsymbol{r}}_1^\top(\boldsymbol{a}(0) + \boldsymbol{w}_1(0)) - \frac{(\hat{\boldsymbol{r}}_1^\top\boldsymbol{w}_2(0))^2}{\hat{\boldsymbol{r}}_1^\top(\boldsymbol{a}(0) + \boldsymbol{w}_1(0))}\right], \qquad w_2(0) = \hat{\boldsymbol{r}}_1^\top\boldsymbol{w}_2(0). \tag{18}$$

Then, there exists a constant $C > 0$, independent of s, such that for all $t \geq 0$, the trajectories $\boldsymbol{a}(t)$, $\boldsymbol{w}_1(t)$, and $\boldsymbol{w}_2(t)$ of the exact gradient flow defined in Equations (9), (10) and (12) are well-approximated by the solution (w_1, w_2), with the approximation error satisfying

$$\left\|\boldsymbol{a}(t) - \hat{\boldsymbol{r}}_1\sqrt{w_1(t)^2 + w_2(t)^2}\right\| \leq Cs, \quad \|\boldsymbol{w}_1(t) - \hat{\boldsymbol{r}}_1 w_1(t)\| \leq Cs, \quad \|\boldsymbol{w}_2(t) - \hat{\boldsymbol{r}}_1 w_2(t)\| \leq Cs. \tag{19}$$

The proof of Theorem 3.3 is provided in detail in Appendix B.4. While random initialization generally introduces an $O(s^2)$ discrepancy between $a(t)^2$ and $w_1(t)^2 + w_2(t)^2$, Equations (16) and (17) seem to describe the dynamics under the exact relationship $a(t)^2 = w_1(t)^2 + w_2(t)^2$. As rigorously shown in Appendix B.4 , the validity of this description relies on the initialization given in Equation (18). These initial conditions are constructed so that the initial discrepancy is confined entirely to the decaying mode $(\boldsymbol{a} - \boldsymbol{w}_1)/2$, while the exponentially growing mode $(\boldsymbol{a} + \boldsymbol{w}_1)/2$ is preserved exactly. As a result, the approximation error does not amplify during the early phase.

3.2.2 Two-Phase Learning Dynamics

We now analyze the learning dynamics of the network using the reduced dynamics established in Theorem 3.3 . Since these reduced dynamics track the high-dimensional trajectory up to an $O(s)$ error, analyzing them is sufficient to understand the actual network behavior.

Early Phase. Starting from the small initialization, w_1 grows exponentially as shown in Lemma 3.1. While Atanasov et al. (2022) identified this initial alignment along the direction of $\boldsymbol{v}_1$ using a linearized multivariate system , the subsequent temporal evolution of the weight magnitude under anisotropic data was not fully explored.

To characterize this evolution, we must examine the behavior of the component w_2. As established in the following proposition, the growth of w_2 is strictly bounded by w_1^3. This guarantees that w_1 remains effectively decoupled from w_2, dominating the early phase dynamics.

Formally, we define a constant R satisfying $\|\boldsymbol{\Sigma}_{xy}\| - \lambda_1 R^2 > 0$ and an exit time $T_R = \inf\{t > 0 : w_1^2 + w_2^2 \geq R^2\}$. For the subsequent claims, we restrict our analysis to the interval $t \in [0, T_R)$.

Proposition 3.4. *There exists a constant $C > 0$ such that for all sufficiently small $s > 0$ and all $t \in [0, T_R)$, the following inequality holds:*

$$|w_2(t)| \leq \frac{2\nu\sqrt{1 + (\nu/\lambda_2)^2}}{3(\|\boldsymbol{\Sigma}_{xy}\| - \lambda_1 R^2)}|w_1(t)|^3 + Cs. \tag{20}$$

The proof of Proposition 3.4 is in Appendix C.1.1. Building on the strong suppression of w_2, we can approximate the evolution of w_1 with a single scalar differential equation :

Proposition 3.5. *For all sufficiently small $s > 0$ and all $t \in [0, T_R)$, the evolution of $w_1(t)$ is governed by*

$$\tau\frac{d}{dt}w_1(t) = \|\boldsymbol{\Sigma}_{xy}\|w_1(t) - \lambda_1 w_1(t)^3 + \varepsilon_R(t) \tag{21}$$

where the remainder $\varepsilon_R(t)$ satisfies $|\varepsilon_R(t)| \leq C_1|w_1(t)|^5 + C_2 s$ for constants $C_1, C_2 > 0$ independent of s.

The proof of Proposition 3.5 is provided in Appendix C.1.2. As long as w_1 has not reached a significant magnitude, the residual $\varepsilon_R(t)$ remains suppressed, effectively decoupling the dynamics of w_1 from the other variables. Solving this truncated equation yields the following sigmoidal growth:

$$w_1(t) \approx \sqrt{\frac{\|\boldsymbol{\Sigma}_{xy}\|}{\left(1 - e^{-2\|\boldsymbol{\Sigma}_{xy}\|t/\tau} + \frac{\|\boldsymbol{\Sigma}_{xy}\|}{\lambda_1}w_1(0)^{-2}e^{-2\|\boldsymbol{\Sigma}_{xy}\|t/\tau}\right)\lambda_1}}. \tag{22}$$

The term $\frac{\|\boldsymbol{\Sigma}_{xy}\|}{\lambda_1}w_1(0)^{-2}e^{-2\|\boldsymbol{\Sigma}_{xy}\|t/\tau}$ in the denominator initially dominates the expression due to the small initial value $w_1(0) = O(s)$. As the exponential factor decays, this term diminishes rapidly, causing $w_1(t)$ to transition sharply from its initial $O(s)$ scale to its $O(1)$ saturation value, approximately $\sqrt{\|\boldsymbol{\Sigma}_{xy}\|/\lambda_1}$.

Equation (22) reveals that, ignoring the residual $\varepsilon_R(t)$, the magnitude evolves according to the same sigmoidal law governing isotropic data. This observation suggests that the anisotropy primarily determines the alignment direction, while the growth dynamics of the magnitude in this phase effectively follow the isotropic case along that direction.

This sigmoidal shape and its characteristic timescale, $\frac{\tau}{2\|\boldsymbol{\Sigma}_{xy}\|}\log(\|\boldsymbol{\Sigma}_{xy}\|/(\lambda_1 s^2))$, are visually confirmed in Figure 2. This implies that learning in this phase becomes faster as $\|\boldsymbol{\Sigma}_{xy}\| = \sigma^2\sqrt{1 + ((1+\rho)^2 - 1)A^2}$ increases, which occurs with a larger spike magnitude ρ and greater alignment A between the spike direction and the target vector.

Later Phase. Next, we examine the phase that occurs once w_1 approaches saturation. As w_1 nears saturation, the upper bound for w_2 established in Proposition 3.4 becomes less restrictive. In general anisotropic settings where the target vector $\boldsymbol{\beta}$ is neither perfectly aligned with nor orthogonal to the spike direction $\boldsymbol{\mu}$ $(0 < A < 1)$, the network must adjust its weights to capture the target using a component other than w_1. The growth of the second component w_2 is driven by the coupling term ν, which is non-zero only under this alignment condition and when the data is anisotropic ($\rho > 0$).

Conversely, if these conditions are not met (i.e., if $A = 0$, $A = 1$, or $\rho = 0$), the term ν vanishes . As seen from Equation (17), w_2 does not grow beyond its initial $O(s)$ magnitude in these cases. In such simpler cases, the learning dynamics are fully described by the early phase alone, a scenario that has been extensively studied (Saxe et al., 2013; Fukumizu, 1998; Atanasov et al., 2022).

While the coupled differential equations for w_1 and w_2 are analytically intractable, we can estimate the time required for w_2 to grow to a substantial fraction of its final value.

Proposition 3.6. *Let $w_{1\infty} = \lim_{t\to\infty} w_1(t)$ and $w_{2\infty} = \lim_{t\to\infty} w_2(t)$, and assume the trajectories satisfy $w_1(t) \geq w_{1\infty}$ and $w_2(t) \leq w_{2\infty}$. Let t_1 denote the time at which $w_2(t)$ first reaches a macroscopic threshold $\varepsilon > 0$. Furthermore, for any $\delta > 0$, let t_2 be the time when $w_2(t)$ reaches $(1 - e^{-\delta})w_{2\infty}$. Then, the duration of this later phase $t_2 - t_1$ is bounded above by*

$$t_2 - t_1 \leq \frac{\tau}{\lambda_2}\left[\frac{\nu}{\lambda_2}\arctan\left(\frac{\nu}{\lambda_2}(1 - e^{-\delta})\right) + \frac{1}{2}\log\left(1 + \left(\frac{\nu}{\lambda_2}(1 - e^{-\delta})\right)^2\right) + \delta\right]. \tag{23}$$

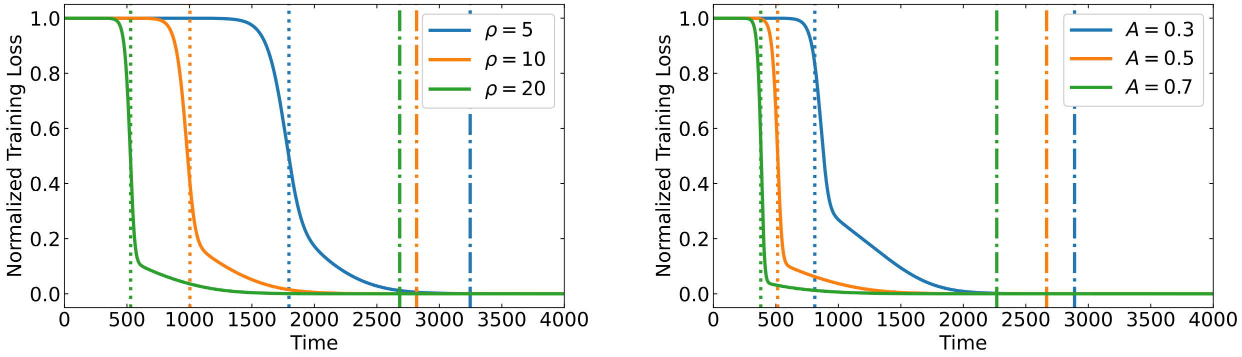

(a) Varying ρ while keeping $A = 0.5$ fixed.

(b) Varying A while keeping $\rho = 20$ fixed.

Figure 3: Evolution of the normalized training loss for different settings of (a) spike magnitude ρ and (b) spike-target alignment A. The loss $\mathcal{L}$ is normalized by the empirical second moment of the labels, $\frac{1}{n}\sum_{i=1}^{n} y_i^2$. Vertical dotted and dash-dotted lines indicate the characteristic timescales for the early and later learning phases, respectively, with the latter defined in Inequality (23) using $\delta = 3$. Other parameters are the same as in Figure 1.

This bound is tight if w_1 changes little during the growth of w_2. The analysis of the timescale highlights that the speed of the later phase is governed by $1/\lambda_2$, representing the inverse of data variance along the $\boldsymbol{v}_2$ direction. The proof of Proposition 3.6 can be found in Appendix C.2.

Figure 2 also shows the later-phase dynamics, as the projection $\hat{\boldsymbol{r}}_1^\top \boldsymbol{W} \boldsymbol{v}_2$ (corresponding to w_2 in the reduced dynamics) begins to grow after $\hat{\boldsymbol{r}}_1^\top \boldsymbol{W} \boldsymbol{v}_1$ (corresponding to w_1) has nearly saturated. Furthermore, the characteristic timescale t_2 derived in Inequality (23), marked by a vertical dash-dotted line, coincides well with the saturation of the w_2 component, validating the theoretical analysis.

The effects of spike magnitude ρ and spike-target alignment A on the training loss are summarized in Figure 3. As shown in the figure, the learning process indeed consists of two phases, with the acceleration in the early phase being the dominant factor shaping the overall training trajectory. This dominance of the early phase, which is more pronounced for a larger spike magnitude ρ and stronger spike-target alignment A, leads to a substantial initial loss reduction and keeps the training loss consistently lower throughout the process. Conversely, when these parameters are small, the loss decreases more slowly, and it becomes difficult to distinguish between the two phases. The theory developed here explains these observations by showing how anisotropic data structures, namely, spike magnitude ρ and spike-target alignment A, influence the two learning phases. A larger spike magnitude ρ primarily accelerates the early phase by increasing the magnitude of the input-output correlation $\|\boldsymbol{\Sigma}_{xy}\|$, while a stronger spike-target alignment A achieves this by slowing the convergence of the later phase through a reduction of λ_2, i.e., the data variance along the direction of $\boldsymbol{v}_2$.

4 Generalization Error under Spiked Covariance Model

We now investigate how the spiked covariance structure affects the generalization performance. While the behavior of generalization error is well-established for isotropic data, its precise dependence on the key parameters of an anisotropic structure, in particular the spike magnitude ρ and spike-target alignment A, has not been fully characterized. This section provides a quantitative analysis of this relationship by deriving a precise analytical expression for the generalization error. Our result explicitly demonstrates this connection, offering a clear theoretical explanation for how these structural properties of data influence generalization.

We focus on the high-dimensional regime where the number of samples n and the data dimension d are large, specifically when $n, d \to \infty$ such that their ratio $\gamma = d/n > 1$. Under this condition, the regression problem admits infinitely many solutions that achieve the optimal training loss. It is known that for high-dimensional regression, linear networks trained with gradient flow from a small initialization converge to a solution close to the minimum ℓ_2-norm solution given by:

$$\hat{\boldsymbol{\beta}}_0 = \boldsymbol{X}^\top (\boldsymbol{X}\boldsymbol{X}^\top)^+ \boldsymbol{y}, \tag{24}$$

where $\boldsymbol{X} \in \mathbb{R}^{n\times d}$ is the design matrix whose rows are the input data $\boldsymbol{x}_i$, and $\boldsymbol{y} \in \mathbb{R}^n$ is the vector of corresponding outputs y_i (Min et al., 2021; Yun et al., 2021).

This solution is also identical to that obtained by ridgeless regression, which corresponds to taking the limit $\lambda \to 0^+$ in ridge regression:

$$\begin{aligned}\hat{\boldsymbol{\beta}}_\lambda &= \arg\min_{\boldsymbol{\beta}} \frac{1}{n}\sum_{i=1}^{n}(y_i - \boldsymbol{\beta}^\top \boldsymbol{x}_i)^2 + \lambda \|\boldsymbol{\beta}\|^2 \\ &= (\boldsymbol{X}^\top \boldsymbol{X} + \lambda n \boldsymbol{I})^{-1}\boldsymbol{X}^\top \boldsymbol{y}.\end{aligned} \tag{25}$$

Therefore, the generalization error of the solution $R_0 = \mathbb{E}[(\hat{\boldsymbol{\beta}}_0^\top \boldsymbol{x} - \boldsymbol{\beta}^\top \boldsymbol{x})^2]$ can be evaluated by taking the ridgeless limit of the ridge regression error

$$R_\lambda = \mathbb{E}[(\hat{\boldsymbol{\beta}}_\lambda^\top \boldsymbol{x} - \boldsymbol{\beta}^\top \boldsymbol{x})^2]. \tag{26}$$

In the high-dimensional limit, recent advances in random matrix theory (Wei et al., 2022; Hastie et al., 2022; Canatar et al., 2021; Wu & Xu, 2020; Richards et al., 2021; Mel & Ganguli, 2021; Atanasov et al., 2024) establish that R_λ converges to:

$$\hat{R}_\lambda = \frac{\partial \kappa(\lambda)}{\partial \lambda}\kappa(\lambda)^2 \sum_{i=1}^{d} \frac{\lambda_i}{(\kappa(\lambda)+\lambda_i)^2}(\boldsymbol{\beta}^\top \boldsymbol{u}_i)^2, \tag{27}$$

where $\boldsymbol{u}_i$ and λ_i are the eigenvectors and eigenvalues of the covariance matrix of the input data, $\boldsymbol{\Sigma} = \sum_{i=1}^{d} \lambda_i \boldsymbol{u}_i \boldsymbol{u}_i^\top$, and $\kappa(\lambda)$ is the unique positive solution of:

$$1 = \frac{\lambda}{\kappa(\lambda)} + \frac{1}{n}\sum_{i=1}^{d}\frac{\lambda_i}{\kappa(\lambda)+\lambda_i}. \tag{28}$$

The final generalization error for the minimum ℓ_2-norm solution is then determined by the limit $\hat{R}_0 = \lim_{\lambda\to 0^+} \hat{R}_\lambda$. By specializing this framework to the spiked covariance model, we can explicitly quantify the impact of data anisotropy on the generalization error:

Theorem 4.1. *Assume the high-dimensional limit $d, n \to \infty$ with $d/n \to \gamma > 1$, and let $\boldsymbol{\Sigma} = \sigma^2(\boldsymbol{I} + \rho\boldsymbol{\mu}\boldsymbol{\mu}^\top)$ and $A = \boldsymbol{\mu}^\top\boldsymbol{\beta}$. Then, for a two-layer linear network trained via gradient flow (Equations* (6) *and* (7)*) under the initialization scale $s \to 0$, the generalization error converges almost surely to:*

$$\hat{R}_0 = \sigma^2\left(1-\frac{1}{\gamma}\right)\left[1 - A^2\left(1 - \frac{1+\rho}{(1+\rho/\gamma)^2}\right)\right]. \tag{29}$$

Proof sketch. The spiked covariance matrix $\boldsymbol{\Sigma}$ has a pricipal eigenvalue $\lambda_1 = \sigma^2(1+\rho)$ corresponding to the spike direction $\boldsymbol{u}_1 = \boldsymbol{\mu}$, while the remaining $d-1$ eigenvalues are $\lambda_i = \sigma^2$. Thus, the spectral distribution of $\boldsymbol{\Sigma}$ is $\frac{1}{d}\delta_{\sigma^2(1+\rho)} + \frac{d-1}{d}\delta_{\sigma^2}$.

In the high-dimensional limit where $n, d \to \infty$ with $d/n \to \gamma$, the contribution of the single spike to the sum $\frac{1}{n}\sum_{i=1}^{d}\frac{\lambda_i}{\kappa(\lambda)+\lambda_i} = \frac{\gamma}{d}\sum_{i=1}^{d}\frac{\lambda_i}{\kappa(\lambda)+\lambda_i}$ vanishes, as its weight $1/d$ becomes negligible. Consequently, the sum is dominated by the $d-1$ isotropic eigenvalues σ^2 . The implicit equation for $\kappa(\lambda)$ then asymptotically reduces to:

$$1 = \frac{\lambda}{\kappa(\lambda)} + \gamma\frac{\sigma^2}{\kappa(\lambda)+\sigma^2}. \tag{30}$$

Taking the limit $\lambda \to 0^+$ and differentiating the implicit equation with respect to λ, we obtain

$$\lim_{\lambda\to 0^+}\kappa(\lambda) = \sigma^2(\gamma-1) \quad \text{and} \quad \lim_{\lambda\to 0^+}\frac{\partial\kappa(\lambda)}{\partial\lambda} = \frac{\gamma}{\gamma-1}. \tag{31}$$

Now, since $A = \boldsymbol{\mu}^\top \boldsymbol{\beta}$, we can decompose the target vector as $\boldsymbol{\beta} = A\boldsymbol{\mu} + \sqrt{1 - A^2}\boldsymbol{u}_2$, where we choose $\boldsymbol{u}_2 = (\boldsymbol{I} - \boldsymbol{\mu}\boldsymbol{\mu}^\top)\boldsymbol{\beta}/\|(\boldsymbol{I} - \boldsymbol{\mu}\boldsymbol{\mu}^\top)\boldsymbol{\beta}\|$ as one of the eigenvectors of $\boldsymbol{\Sigma}$ orthogonal to $\boldsymbol{\mu}$. Substituting this decomposition, along with Equation (31), into Equation (27) gives the generalization error . □

The full proof of Theorem 4.1 can be found in Appendix D. Note that this expression with $\rho = 0$ recovers previous results for isotropic data (Mei & Montanari, 2022; Belkin et al., 2020). To better assess the performance of the model relative to the signal strength, we evaluate the normalized generalization error, which is the error $\hat{R}_0$ divided by the variance of the true signal, $\mathbb{E}[y^2] = \boldsymbol{\beta}^\top \boldsymbol{\Sigma} \boldsymbol{\beta} = \sigma^2(1 + \rho A^2)$. Our analysis predicts that this normalized error $\hat{R}_0/\mathbb{E}[y^2]$ is minimized when the spike magnitude ρ is large and spike-target alignment A is strong . This indicates that a pronounced anisotropy of the data structure significantly improves generalization if the anisotropy, represented by the spike, is suitably aligned with the direction of the target vector of the task. Conversely, when the target signal is orthogonal to the spike ($A = 0$), the spike provides no benefit to generalization performance. This overall theoretical dependence of the normalized error on both spike magnitude and spike-target alignment is shown in Figure 4.

To validate these theoretical predictions, we conducted numerical simulations of a two-layer linear network with small initialization, illustrated in Figure 5. The results show a close match between the empirical normalized generalization errors and the theoretical predictions across a range of parameters.

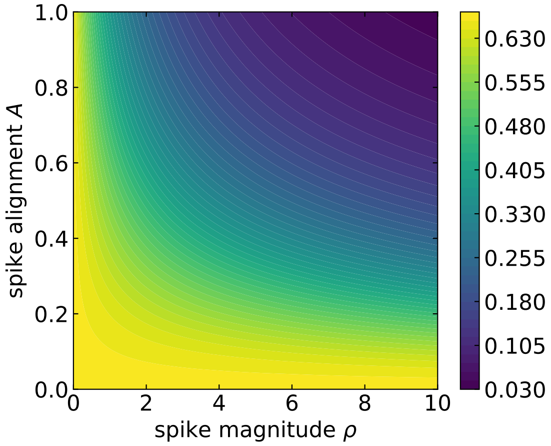

Figure 4: Normalized generalization error $\hat{R}_0/\boldsymbol{\beta}^\top \boldsymbol{\Sigma} \boldsymbol{\beta}$ as a function of spike-target alignment A and spike magnitude ρ for a fixed ratio $\gamma = 3$.

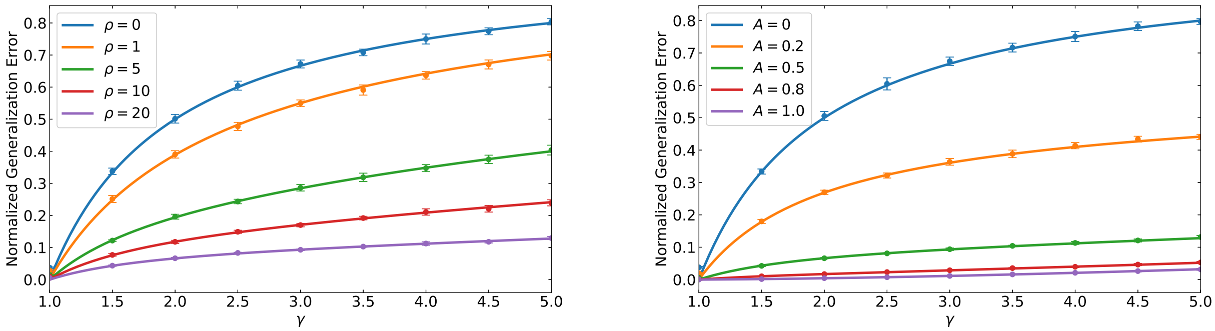

(a) Varying ρ while keeping $A = 0.5$ fixed.

(b) Varying A while keeping $\rho = 20$ fixed.

Figure 5: Normalized generalization error $\hat{R}_0/\boldsymbol{\beta}^\top \boldsymbol{\Sigma} \boldsymbol{\beta}$ as a function of the ratio $\gamma = d/n$. Solid lines represent the theoretical prediction (Equation (29)) and points are results of numerical simulations. The empirical results are averaged over 10 independent trials, with error bars indicating the standard deviation. All simulations were performed with a two-layer linear network of input dimension $d = 3000$ and width $m = 3000$, with $\sigma^2 = 1$. The initialization procedure is the same as in Figure 1.

5 Discussion and Conclusion

In this work, we investigated the learning dynamics of two-layer linear networks trained on data with a spiked covariance structure and analyzed the resulting generalization error. Theoretical analysis revealed several key insights into how data anisotropy shapes the learning process and generalization.

First, we characterized the learning dynamics, revealing two distinct phases. The early phase involves rapid weight growth in the direction of the input-output correlation $\boldsymbol{v}_1$. The speed of this phase, proportional to $\|\boldsymbol{\Sigma}_{xy}\|$, increases with both a larger spike magnitude and a stronger spike-target alignment. Once this component saturates, the later phase begins. During this phase, learning along the direction $\boldsymbol{v}_2$, which is defined within the span of $\{\boldsymbol{\Sigma}_{xy}, \boldsymbol{\beta}\}$ and orthogonal to $\boldsymbol{v}_1$, becomes significant. Its growth rate is governed by $\lambda_2 = \boldsymbol{v}_2^\top \boldsymbol{\Sigma} \boldsymbol{v}_2$ under the condition that the component in the $\boldsymbol{v}_1$ direction decreases during the later phase. The analysis of the dynamics in this data-adapted basis reveals a mechanism behind these two phases. By decomposing weight evolution along these axes, we obtain a reduced-dimensionality model that clearly explains how the network learns features in phases.

Second, we derived an analytical expression for the generalization error in the high-dimensional regime where $d, n \to \infty$ with $d/n = \gamma > 1$. The expression (Equation (29)) quantifies the dependence of the error on the spike magnitude and the spike-target alignment. Our analysis shows that a larger, well-aligned spike leads to lower generalization error, confirming the benefit of prominent, task-relevant data features. This result extends previous work on isotropic data by quantifying the impact of the spiked covariance structure, a fundamental model of data anisotropy.

Our findings connect to and extend several lines of prior research. While the dynamics of linear networks on isotropic data are well-understood (Fukumizu, 1998; Saxe et al., 2013; 2019; Braun et al., 2022; Dominé et al., 2024), and the initial alignment phase under small initialization has been previously identified (Atanasov et al., 2022), our work investigates the later phases of learning under a specific anisotropic model. This provides a more complete picture of how different components of the solution are learned over time. The generalization error analysis complements previous works (Hastie et al., 2022; Wu & Xu, 2020; Richards et al., 2021; Mel & Ganguli, 2021) by providing concrete expressions for the spiked model, making the effects of anisotropy explicit.

However, our study has several limitations. The analysis is restricted to two-layer linear networks, and the spiked covariance model represents only a specific form of anisotropy. Additionally, the theory developed here employs small initialization, leaving the effects of varying initialization scales between layers unexplored. Furthermore, the dynamics analysis assumes a finite dimension d with an infinite number of samples ($n \to \infty$), whereas the generalization analysis is performed in the high-dimensional limit where $d, n \to \infty$ with their ratio held constant.

These limitations suggest several directions for future research. A direct extension of our work would involve generalizing the analysis to non-linear activations and deeper architectures. Based on our findings, another valuable direction would be to investigate learning dynamics under more complex anisotropic structures, such as multiple spikes or power-law spectral densities that are ubiquitous in natural datasets. Moreover, reconciling our dynamics and generalization analyses within a unified theoretical framework remains a significant problem. Finally, a crucial next step is to explore practical strategies, such as initialization schemes, learning rate schedules, and optimization algorithms, that explicitly exploit data anisotropy to achieve faster convergence and lower generalization error.

In conclusion, this work provides a theoretical perspective on the relationship between data anisotropy, learning dynamics, and generalization in linear networks. By analyzing how a simple anisotropic structure influences learning phases and the final performance, we contribute to a deeper understanding of the mechanisms that shape learning in structured data environments.

References

Ben Adlam and Jeffrey Pennington. The neural tangent kernel in high dimensions: Triple descent and a multi-scale theory of generalization. In *International Conference on Machine Learning*, pp. 74–84. PMLR, 2020.

Madhu S Advani, Andrew M Saxe, and Haim Sompolinsky. High-dimensional dynamics of generalization error in neural networks. *Neural Networks*, 132:428–446, 2020.

Sanjeev Arora, Nadav Cohen, Noah Golowich, and Wei Hu. A convergence analysis of gradient descent for deep linear neural networks. *arXiv preprint arXiv:1810.02281*, 2018.

Sanjeev Arora, Nadav Cohen, Wei Hu, and Yuping Luo. Implicit regularization in deep matrix factorization. *Advances in Neural Information Processing Systems*, 32, 2019.

Alexander Atanasov, Blake Bordelon, and Cengiz Pehlevan. Neural networks as kernel learners: The silent alignment effect. In *International Conference on Learning Representations*, 2022.

Alexander Atanasov, Jacob A Zavatone-Veth, and Cengiz Pehlevan. Scaling and renormalization in high-dimensional regression. *arXiv preprint arXiv:2405.00592*, 2024.

Pierre Baldi and Kurt Hornik. Neural networks and principal component analysis: Learning from examples without local minima. *Neural networks*, 2(1):53–58, 1989.

Peter L Bartlett, Philip M Long, Gábor Lugosi, and Alexander Tsigler. Benign overfitting in linear regression. *Proceedings of the National Academy of Sciences*, 117(48):30063–30070, 2020.

Mikhail Belkin, Daniel Hsu, and Ji Xu. Two models of double descent for weak features. *SIAM Journal on Mathematics of Data Science*, 2(4):1167–1180, 2020.

Lukas Braun, Clémentine Dominé, James Fitzgerald, and Andrew Saxe. Exact learning dynamics of deep linear networks with prior knowledge. *Advances in Neural Information Processing Systems*, 35:6615–6629, 2022.

Abdulkadir Canatar, Blake Bordelon, and Cengiz Pehlevan. Spectral bias and task-model alignment explain generalization in kernel regression and infinitely wide neural networks. *Nature communications*, 12(1): 2914, 2021.

Clémentine CJ Dominé, Nicolas Anguita, Alexandra M Proca, Lukas Braun, Daniel Kunin, Pedro AM Mediano, and Andrew M Saxe. From lazy to rich: Exact learning dynamics in deep linear networks. *arXiv preprint arXiv:2409.14623*, 2024.

Simon Du and Wei Hu. Width provably matters in optimization for deep linear neural networks. In *International Conference on Machine Learning*, pp. 1655–1664. PMLR, 2019.

Kenji Fukumizu. Effect of batch learning in multilayer neural networks. In *International Conference on Neural Information Processing*, 1998.

Gauthier Gidel, Francis Bach, and Simon Lacoste-Julien. Implicit regularization of discrete gradient dynamics in linear neural networks. *Advances in Neural Information Processing Systems*, 32, 2019.

Suriya Gunasekar, Blake E Woodworth, Srinadh Bhojanapalli, Behnam Neyshabur, and Nati Srebro. Implicit regularization in matrix factorization. *Advances in neural information processing systems*, 30, 2017.

Suriya Gunasekar, Jason D Lee, Daniel Soudry, and Nati Srebro. Implicit bias of gradient descent on linear convolutional networks. *Advances in neural information processing systems*, 31, 2018.

Trevor Hastie, Andrea Montanari, Saharon Rosset, and Ryan J Tibshirani. Surprises in high-dimensional ridgeless least squares interpolation. *Annals of statistics*, 50(2):949, 2022.

Dongsung Huh. Curvature-corrected learning dynamics in deep neural networks. In *International Conference on Machine Learning*, pp. 4552–4560. PMLR, 2020.

Ziwei Ji and Matus Telgarsky. Gradient descent aligns the layers of deep linear networks. *arXiv preprint arXiv:1810.02032*, 2018.

Iain M Johnstone. On the distribution of the largest eigenvalue in principal components analysis. *The Annals of statistics*, 29(2):295–327, 2001.

Hassan K Khalil. *Nonlinear systems.* Prentice Hall, Upper Saddle River, NJ, 3rd edition, 2002.

Daniel Kunin, Atsushi Yamamura, Chao Ma, and Surya Ganguli. The asymmetric maximum margin bias of quasi-homogeneous neural networks. In *The Eleventh International Conference on Learning Representations*, 2023.

Daniel Kunin, Allan Raventos, Clémentine Carla Juliette Dominé, Feng Chen, David Klindt, Andrew M Saxe, and Surya Ganguli. Get rich quick: exact solutions reveal how unbalanced initializations promote rapid feature learning. In *The Thirty-eighth Annual Conference on Neural Information Processing Systems*, 2024.

Andrew K Lampinen and Surya Ganguli. An analytic theory of generalization dynamics and transfer learning in deep linear networks. *arXiv preprint arXiv:1809.10374*, 2018.

Pierre Marion and Lénaïc Chizat. Deep linear networks for regression are implicitly regularized towards flat minima. *arXiv preprint arXiv:2405.13456*, 2024.

Song Mei and Andrea Montanari. The generalization error of random features regression: Precise asymptotics and the double descent curve. *Communications on Pure and Applied Mathematics*, 75(4):667–766, 2022.

Gabriel Mel and Surya Ganguli. A theory of high dimensional regression with arbitrary correlations between input features and target functions: sample complexity, multiple descent curves and a hierarchy of phase transitions. In *International Conference on Machine Learning*, pp. 7578–7587. PMLR, 2021.

Gabriel Mel and Jeffrey Pennington. Anisotropic random feature regression in high dimensions. In *International Conference on Learning Representations*, 2021.

Hancheng Min, Salma Tarmoun, René Vidal, and Enrique Mallada. On the explicit role of initialization on the convergence and implicit bias of overparametrized linear networks. In *International Conference on Machine Learning*, pp. 7760–7768. PMLR, 2021.

Scott Pesme, Loucas Pillaud-Vivien, and Nicolas Flammarion. Implicit bias of sgd for diagonal linear networks: a provable benefit of stochasticity. *Advances in Neural Information Processing Systems*, 34: 29218–29230, 2021.

Mohammad Pezeshki, Amartya Mitra, Yoshua Bengio, and Guillaume Lajoie. Multi-scale feature learning dynamics: Insights for double descent. In *International Conference on Machine Learning*, pp. 17669–17690. PMLR, 2022.

Tomaso Poggio, Qianli Liao, Brando Miranda, Andrzej Banburski, Xavier Boix, and Jack Hidary. Theory iiib: Generalization in deep networks. *arXiv preprint arXiv:1806.11379*, 2018.

Dominic Richards, Jaouad Mourtada, and Lorenzo Rosasco. Asymptotics of ridge (less) regression under general source condition. In *International Conference on Artificial Intelligence and Statistics*, pp. 3889–3897. PMLR, 2021.

Andrew M Saxe, James L McClelland, and Surya Ganguli. Exact solutions to the nonlinear dynamics of learning in deep linear neural networks. *arXiv preprint arXiv:1312.6120*, 2013.

Andrew M Saxe, James L McClelland, and Surya Ganguli. A mathematical theory of semantic development in deep neural networks. *Proceedings of the National Academy of Sciences*, 116(23):11537–11546, 2019.

Haozhe Shan and Blake Bordelon. A theory of neural tangent kernel alignment and its influence on training. *arXiv preprint arXiv:2105.14301*, 2021.

Salma Tarmoun, Guilherme Franca, Benjamin D Haeffele, and Rene Vidal. Understanding the dynamics of gradient flow in overparameterized linear models. In *International Conference on Machine Learning*, pp. 10153–10161. PMLR, 2021.

Aditya Vardhan Varre, Maria-Luiza Vladarean, Loucas Pillaud-Vivien, and Nicolas Flammarion. On the spectral bias of two-layer linear networks. *Advances in Neural Information Processing Systems*, 36:64380–64414, 2023.

Alexander Wei, Wei Hu, and Jacob Steinhardt. More than a toy: Random matrix models predict how real-world neural representations generalize. In *International conference on machine learning*, pp. 23549–23588. PMLR, 2022.

Blake Woodworth, Suriya Gunasekar, Jason D Lee, Edward Moroshko, Pedro Savarese, Itay Golan, Daniel Soudry, and Nathan Srebro. Kernel and rich regimes in overparametrized models. In *Conference on Learning Theory*, pp. 3635–3673. PMLR, 2020.

Denny Wu and Ji Xu. On the optimal weighted ℓ_2 regularization in overparameterized linear regression. *Advances in Neural Information Processing Systems*, 33:10112–10123, 2020.

Chulhee Yun, Shankar Krishnan, and Hossein Mobahi. A unifying view on implicit bias in training linear neural networks. In *International Conference on Learning Representations*, 2021.

Yedi Zhang, Peter E. Latham, and Andrew M Saxe. Understanding unimodal bias in multimodal deep linear networks. In *Forty-first International Conference on Machine Learning*, 2024.

A Derivation of Decomposed Dynamics and Covariance Components

A.1 Derivation of the Decomposed Dynamics

In this subsection, we provide the derivation of the decomposed dynamics (Equations (9) to (12)) used in the main text.

Let $\widetilde{\boldsymbol{\Sigma}}_{xy} = \boldsymbol{V}^\top \boldsymbol{\Sigma}_{xy}$. Then, by construction of the basis $\boldsymbol{V}$, we have $\boldsymbol{v}_1 = \boldsymbol{\Sigma}_{xy}/\|\boldsymbol{\Sigma}_{xy}\|$ and hence $\boldsymbol{\Sigma}_{xy}^\top \boldsymbol{v}_i = 0$ for $i = 2, \ldots, d$. Therefore,

$$\boldsymbol{\Sigma}_{xy}^\top \boldsymbol{V} = (\boldsymbol{\Sigma}_{xy}^\top \boldsymbol{v}_1, \boldsymbol{\Sigma}_{xy}^\top \boldsymbol{v}_2, \ldots, \boldsymbol{\Sigma}_{xy}^\top \boldsymbol{v}_d) = (\|\boldsymbol{\Sigma}_{xy}\|, 0, \ldots, 0). \tag{A.1}$$

Let $\widetilde{\boldsymbol{\Sigma}} := \boldsymbol{V}^\top \boldsymbol{\Sigma} \boldsymbol{V}$. Since the vectors $\{\boldsymbol{v}_3, \ldots, \boldsymbol{v}_d\}$ span the subspace orthogonal to $\mathrm{span}\{\boldsymbol{\Sigma}_{xy}, \boldsymbol{\beta}\}$, and this subspace is an eigenspace of the spiked covariance matrix with eigenvalue σ^2, we have

$$\widetilde{\boldsymbol{\Sigma}} = \begin{pmatrix} \lambda_1 & -\nu & 0 & \cdots & 0 \\ -\nu & \lambda_2 & 0 & \cdots & 0 \\ 0 & 0 & \sigma^2 & & 0 \\ \vdots & \vdots & & \ddots & \vdots \\ 0 & 0 & 0 & \cdots & \sigma^2 \end{pmatrix}, \tag{A.2}$$

where $\lambda_1 = \boldsymbol{v}_1^\top \boldsymbol{\Sigma} \boldsymbol{v}_1$, $\lambda_2 = \boldsymbol{v}_2^\top \boldsymbol{\Sigma} \boldsymbol{v}_2$, and $\nu = -\boldsymbol{v}_1^\top \boldsymbol{\Sigma} \boldsymbol{v}_2$.

We also define

$$\widetilde{\boldsymbol{W}} := \boldsymbol{W}\boldsymbol{V} = (\boldsymbol{w}_1, \boldsymbol{w}_2, \ldots, \boldsymbol{w}_d). \tag{A.3}$$

Multiplying Equation (6) on the right by $\boldsymbol{V}$ and using $\boldsymbol{W} = \widetilde{\boldsymbol{W}}\boldsymbol{V}^\top$, $\boldsymbol{\Sigma}_{xy} = \boldsymbol{V}\widetilde{\boldsymbol{\Sigma}}_{xy}$, and $\boldsymbol{\Sigma} = \boldsymbol{V}\widetilde{\boldsymbol{\Sigma}}\boldsymbol{V}^\top$ yields

$$\begin{aligned} \tau \frac{d}{dt}\widetilde{\boldsymbol{W}} &= \tau \frac{d}{dt}(\boldsymbol{W}\boldsymbol{V}) \\ &= \boldsymbol{a}\left(\boldsymbol{\Sigma}_{xy}^\top - \boldsymbol{a}^\top \boldsymbol{W}\boldsymbol{\Sigma}\right)\boldsymbol{V} \\ &= \boldsymbol{a}\left(\boldsymbol{\Sigma}_{xy}^\top \boldsymbol{V} - \boldsymbol{a}^\top \widetilde{\boldsymbol{W}}\boldsymbol{V}^\top \boldsymbol{\Sigma}\boldsymbol{V}\right) \\ &= \boldsymbol{a}\left(\widetilde{\boldsymbol{\Sigma}}_{xy}^\top - \boldsymbol{a}^\top \widetilde{\boldsymbol{W}}\widetilde{\boldsymbol{\Sigma}}\right). \end{aligned} \tag{A.4}$$

Since $\widetilde{\boldsymbol{W}} = (\boldsymbol{w}_1, \boldsymbol{w}_2, \dots, \boldsymbol{w}_d)$, taking the i-th column gives

$$\tau \frac{d}{dt}\boldsymbol{w}_i = \boldsymbol{a}\left((\widetilde{\boldsymbol{\Sigma}}_{xy})_i - (\widetilde{\boldsymbol{\Sigma}}\widetilde{\boldsymbol{W}}^\top \boldsymbol{a})_i\right), \tag{A.5}$$

where $(\widetilde{\boldsymbol{\Sigma}}_{xy})_i$ and $(\widetilde{\boldsymbol{\Sigma}}\widetilde{\boldsymbol{W}}^\top \boldsymbol{a})_i$ denote the i-th entries of $\widetilde{\boldsymbol{\Sigma}}_{xy}$ and $\widetilde{\boldsymbol{\Sigma}}\widetilde{\boldsymbol{W}}^\top \boldsymbol{a}$, respectively.

Using $\widetilde{\boldsymbol{\Sigma}}_{xy} = (\|\boldsymbol{\Sigma}_{xy}\|, 0, \dots, 0)^\top$ and $\widetilde{\boldsymbol{W}}^\top \boldsymbol{a} = (\boldsymbol{a}^\top \boldsymbol{w}_1, \dots, \boldsymbol{a}^\top \boldsymbol{w}_d)^\top$, together with the block structure of $\widetilde{\boldsymbol{\Sigma}}$, we obtain Equations (9) to (11):

$$\begin{aligned}
\tau \frac{d}{dt}\boldsymbol{w}_1 &= \|\boldsymbol{\Sigma}_{xy}\|\boldsymbol{a} - (\lambda_1 \boldsymbol{a}^\top \boldsymbol{w}_1 - \nu \boldsymbol{a}^\top \boldsymbol{w}_2)\boldsymbol{a}, && \text{(A.6)}\\
\tau \frac{d}{dt}\boldsymbol{w}_2 &= -(-\nu \boldsymbol{a}^\top \boldsymbol{w}_1 + \lambda_2 \boldsymbol{a}^\top \boldsymbol{w}_2)\boldsymbol{a}, && \text{(A.7)}\\
\tau \frac{d}{dt}\boldsymbol{w}_i &= -\sigma^2 \boldsymbol{a}^\top \boldsymbol{w}_i \boldsymbol{a}, \qquad (i = 3, \dots, d). && \text{(A.8)}
\end{aligned}$$

Similarly, using Equation (7), we obtain

$$\begin{aligned}
\tau \frac{d}{dt}\boldsymbol{a}^\top &= \left(\boldsymbol{\Sigma}_{xy}^\top - \boldsymbol{a}^\top \boldsymbol{W}\boldsymbol{\Sigma}\right)\boldsymbol{W}^\top\\
&= \left(\widetilde{\boldsymbol{\Sigma}}_{xy}^\top \boldsymbol{V}^\top - \boldsymbol{a}^\top \widetilde{\boldsymbol{W}}\boldsymbol{V}^\top \boldsymbol{V}\widetilde{\boldsymbol{\Sigma}}\boldsymbol{V}^\top\right)\boldsymbol{V}\widetilde{\boldsymbol{W}}^\top\\
&= \left(\widetilde{\boldsymbol{\Sigma}}_{xy}^\top - \boldsymbol{a}^\top \widetilde{\boldsymbol{W}}\widetilde{\boldsymbol{\Sigma}}\right)\widetilde{\boldsymbol{W}}^\top
\end{aligned} \tag{A.9}$$

Taking the transpose and expanding in terms of $\widetilde{\boldsymbol{W}} = (\boldsymbol{w}_1, \dots, \boldsymbol{w}_d)$ gives

$$\tau \frac{d}{dt}\boldsymbol{a} = \widetilde{\boldsymbol{W}}\left(\widetilde{\boldsymbol{\Sigma}}_{xy} - \widetilde{\boldsymbol{\Sigma}}\widetilde{\boldsymbol{W}}^\top \boldsymbol{a}\right) = \sum_{i=1}^{d} \boldsymbol{w}_i \left((\widetilde{\boldsymbol{\Sigma}}_{xy})_i - (\widetilde{\boldsymbol{\Sigma}}\widetilde{\boldsymbol{W}}^\top \boldsymbol{a})_i\right). \tag{A.10}$$

Substituting as before, we obtain Equation (12):

$$\tau \frac{d}{dt}\boldsymbol{a} = \|\boldsymbol{\Sigma}_{xy}\|\boldsymbol{w}_1 - (\lambda_1 \boldsymbol{a}^\top \boldsymbol{w}_1 - \nu \boldsymbol{a}^\top \boldsymbol{w}_2)\boldsymbol{w}_1 - (-\nu \boldsymbol{a}^\top \boldsymbol{w}_1 + \lambda_2 \boldsymbol{a}^\top \boldsymbol{w}_2)\boldsymbol{w}_2 - \sum_{i=3}^{d} \sigma^2 \boldsymbol{a}^\top \boldsymbol{w}_i\, \boldsymbol{w}_i. \tag{A.11}$$

A.2 Derivation of Input-Output Correlation and Input Covariance Components

In this subsection, we provide detailed derivations for the quantities related to the correlation between the spike and the target signal, discussed in the main text. We use the notation $A = \boldsymbol{\mu}^\top \boldsymbol{\beta}$.

First, we calculate the norm of the input-output correlation $\boldsymbol{\Sigma}_{xy}$. Using Equation (1) and Equation (3), we can derive it as follows:

$$\begin{aligned}
\|\boldsymbol{\Sigma}_{xy}\| &= \|\sigma^2(\boldsymbol{I} + \rho\boldsymbol{\mu}\boldsymbol{\mu}^\top)\boldsymbol{\beta}\|\\
&= \sigma^2\sqrt{1 + 2\rho A^2 + \rho^2 A^2}\\
&= \sigma^2\sqrt{1 + ((1+\rho)^2 - 1)A^2}.
\end{aligned} \tag{A.12}$$

Next, we calculate the components of the input covariance matrix $\boldsymbol{\Sigma}$ in the basis $\{\boldsymbol{v}_1, \boldsymbol{v}_2\}$. These components are the diagonal terms $\lambda_1 = \boldsymbol{v}_1^\top \boldsymbol{\Sigma}\boldsymbol{v}_1$ and $\lambda_2 = \boldsymbol{v}_2^\top \boldsymbol{\Sigma}\boldsymbol{v}_2$, and the off-diagonal term $\nu = -\boldsymbol{v}_1^\top \boldsymbol{\Sigma}\boldsymbol{v}_2$. To compute them, we first need the inner products of the spike direction $\boldsymbol{\mu}$ with the basis vectors.

The inner product between $\boldsymbol{\mu}$ and $\boldsymbol{v}_1$ is computed as follows:

$$\begin{aligned}
\boldsymbol{\mu}^\top \boldsymbol{v}_1 &= \frac{1}{\|\boldsymbol{\Sigma}_{xy}\|}\sigma^2 \boldsymbol{\mu}^\top (\boldsymbol{I} + \rho\boldsymbol{\mu}\boldsymbol{\mu}^\top)\boldsymbol{\beta}\\
&= \frac{(1+\rho)A}{\sqrt{1 + ((1+\rho)^2 - 1)A^2}}.
\end{aligned} \tag{A.13}$$

Since $\|\boldsymbol{\mu}\| = 1$ and $\boldsymbol{v}_1$ and $\boldsymbol{v}_2$ form an orthonormal basis for the relevant subspace, we have $(\boldsymbol{\mu}^\top \boldsymbol{v}_1)^2 + (\boldsymbol{\mu}^\top \boldsymbol{v}_2)^2 = 1$. The inner product of $\boldsymbol{\mu}$ with $\boldsymbol{v}_2$ is then calculated as:

$$\begin{aligned}\boldsymbol{\mu}^\top \boldsymbol{v}_2 &= -\sqrt{1 - (\boldsymbol{\mu}^\top \boldsymbol{v}_1)^2} \\ &= -\sqrt{1 - \frac{(1+\rho)^2 A^2}{1 + ((1+\rho)^2 - 1)A^2}}.\end{aligned} \tag{A.14}$$

Using these inner products, we can now calculate the components of the covariance matrix. The first diagonal component, λ_1, is:

$$\begin{aligned}\lambda_1 &= \boldsymbol{v}_1^\top \boldsymbol{\Sigma} \boldsymbol{v}_1 \\ &= \sigma^2 \boldsymbol{v}_1^\top (\boldsymbol{I} + \rho \boldsymbol{\mu}\boldsymbol{\mu}^\top) \boldsymbol{v}_1 \\ &= \sigma^2 (1 + \rho (\boldsymbol{\mu}^\top \boldsymbol{v}_1)^2) \\ &= \sigma^2 \left[1 + \rho \frac{(1+\rho)^2 A^2}{1 + ((1+\rho)^2 - 1)A^2}\right].\end{aligned} \tag{A.15}$$

Similarly, the second diagonal component, λ_2, is:

$$\begin{aligned}\lambda_2 &= \boldsymbol{v}_2^\top \boldsymbol{\Sigma} \boldsymbol{v}_2 \\ &= \sigma^2 \boldsymbol{v}_2^\top (\boldsymbol{I} + \rho \boldsymbol{\mu}\boldsymbol{\mu}^\top) \boldsymbol{v}_2 \\ &= \sigma^2 (1 + \rho (\boldsymbol{\mu}^\top \boldsymbol{v}_2)^2) \\ &= \sigma^2 \left[1 + \rho \left(1 - \frac{(1+\rho)^2 A^2}{1 + ((1+\rho)^2 - 1)A^2}\right)\right].\end{aligned} \tag{A.16}$$

The off-diagonal term, ν, is calculated as follows:

$$\begin{aligned}\nu &= -\boldsymbol{v}_1^\top \boldsymbol{\Sigma} \boldsymbol{v}_2 \\ &= -\sigma^2 \boldsymbol{v}_1^\top (\boldsymbol{I} + \rho \boldsymbol{\mu}\boldsymbol{\mu}^\top) \boldsymbol{v}_2 \\ &= -\sigma^2 (\boldsymbol{v}_1^\top \boldsymbol{v}_2 + \rho (\boldsymbol{\mu}^\top \boldsymbol{v}_1)(\boldsymbol{\mu}^\top \boldsymbol{v}_2)) \\ &= -\sigma^2 \rho (\boldsymbol{\mu}^\top \boldsymbol{v}_1)(\boldsymbol{\mu}^\top \boldsymbol{v}_2) \\ &= \sigma^2 \rho \frac{(1+\rho) A \sqrt{1 - A^2}}{1 + ((1+\rho)^2 - 1)A^2}.\end{aligned} \tag{A.17}$$

B Dimensionality Reduction to a Two-Variable System

Assumption on the Initialization. Throughout our analysis, we assume that the parameters are initialized at scale s, where $s \ll 1$. Specifically, to ensure that the learning dynamics escape the unstable saddle point at the origin, we focus on non-degenerate initializations where the parameters satisfy the following bounds for some positive constants $\underline{c}$ and $\bar{c}$ independent of s:

$$\underline{c}s \le \|\boldsymbol{a}(0)\| \le \bar{c}s, \quad \underline{c}s \le \|\boldsymbol{w}_i(0)\| \le \bar{c}s \quad (i = 1, \ldots, d). \tag{B.1}$$

Also we assume $\boldsymbol{a}(0) \neq \boldsymbol{w}_1(0)$.

Under Gaussian initialization with standard deviation s, these condition holds almost surely.

Overview of the Dimensionality Reduction Strategy. It is challenging to prove that the approximation error between the full system and the reduced system remains $O(s)$ at all times. This is because the early phase lasts $t = O(\log(1/s))$. Naively applying Gronwall's inequality here yields a divergent bound of

$O(s\exp(O(\log(1/s)))) = O(1)$. To avoid this exponential blow-up, we decouple the growing and decaying modes.

To this end, we introduce the variables $\boldsymbol{u}$ and $\boldsymbol{v}$, which correspond to the growing and decaying modes, respectively, of the linearized $(\boldsymbol{a}, \boldsymbol{w}_1)$ subsystem:

$$\boldsymbol{u} := \frac{\boldsymbol{a} + \boldsymbol{w}_1}{2}, \quad \boldsymbol{v} := \frac{\boldsymbol{a} - \boldsymbol{w}_1}{2}, \tag{B.2}$$

so that $\boldsymbol{a} = \boldsymbol{u} + \boldsymbol{v}$ and $\boldsymbol{w}_1 = \boldsymbol{u} - \boldsymbol{v}$. By the assumption on the initialization, there exist positive constants c_{u0} and c_{v0} such that $\|\boldsymbol{u}(0)\| = c_{u0}s$ and $\|\boldsymbol{v}(0)\| = c_{v0}s$.

From Equations (9) and (12), we obtain

$$\tau\frac{d}{dt}\boldsymbol{u} = \|\boldsymbol{\Sigma}_{xy}\|\boldsymbol{u} + \boldsymbol{e}_u, \tag{B.3}$$

$$\tau\frac{d}{dt}\boldsymbol{v} = -\|\boldsymbol{\Sigma}_{xy}\|\boldsymbol{v} + \boldsymbol{e}_v, \tag{B.4}$$

where

$$\boldsymbol{e}_u := -(\lambda_1\boldsymbol{a}^\top\boldsymbol{w}_1 - \nu\boldsymbol{a}^\top\boldsymbol{w}_2)\boldsymbol{u} - \frac{1}{2}(-\nu\boldsymbol{a}^\top\boldsymbol{w}_1 + \lambda_2\boldsymbol{a}^\top\boldsymbol{w}_2)\boldsymbol{w}_2 - \frac{1}{2}\sum_{i=3}^{d}\sigma^2(\boldsymbol{a}^\top\boldsymbol{w}_i)\boldsymbol{w}_i, \tag{B.5}$$

$$\boldsymbol{e}_v := (\lambda_1\boldsymbol{a}^\top\boldsymbol{w}_1 - \nu\boldsymbol{a}^\top\boldsymbol{w}_2)\boldsymbol{v} - \frac{1}{2}(-\nu\boldsymbol{a}^\top\boldsymbol{w}_1 + \lambda_2\boldsymbol{a}^\top\boldsymbol{w}_2)\boldsymbol{w}_2 - \frac{1}{2}\sum_{i=3}^{d}\sigma^2(\boldsymbol{a}^\top\boldsymbol{w}_i)\boldsymbol{w}_i. \tag{B.6}$$

Applying the variation of constants formula to Equation (B.3) and Equation (B.4), we obtain

$$\boldsymbol{u}(t) = \boldsymbol{u}(0)e^{\|\boldsymbol{\Sigma}_{xy}\|t/\tau} + \frac{1}{\tau}\int_0^t e^{\|\boldsymbol{\Sigma}_{xy}\|(t-t')/\tau}\boldsymbol{e}_u(t')\,dt', \tag{B.7}$$

$$\boldsymbol{v}(t) = \boldsymbol{v}(0)e^{-\|\boldsymbol{\Sigma}_{xy}\|t/\tau} + \frac{1}{\tau}\int_0^t e^{-\|\boldsymbol{\Sigma}_{xy}\|(t-t')/\tau}\boldsymbol{e}_v(t')\,dt'. \tag{B.8}$$

B.1 Initial Alignment and Condensation in the Early Phase (Proof of Lemma 3.1)

In this subsection, we prove Lemma 3.1.

Lemma B.1. *For all* $0 \le t < \frac{2\tau}{3(\|\boldsymbol{\Sigma}_{xy}\| + 2\operatorname{Tr}\boldsymbol{\Sigma})}\log\frac{1}{s}$, *the maximum parameter norm defined as* $X(t) := \max\{\|\boldsymbol{a}(t)\|, \|\boldsymbol{w}_1(t)\|, \|\boldsymbol{w}_2(t)\|, \dots, \|\boldsymbol{w}_d(t)\|\}$ *satisfies the following exponential bound:*

$$X(t) \le X(0)e^{(\|\boldsymbol{\Sigma}_{xy}\| + 2\operatorname{Tr}\boldsymbol{\Sigma})t/\tau}. \tag{B.9}$$

Proof. To analyze the growth of $X(t)$, we first establish bounds the residual error terms. To this end, we can bound terms as:

$$|\lambda_1\boldsymbol{a}^\top\boldsymbol{w}_1 - \nu\boldsymbol{a}^\top\boldsymbol{w}_2| \le \lambda_1\|\boldsymbol{a}\|\|\boldsymbol{w}_1\| + \nu\|\boldsymbol{a}\|\|\boldsymbol{w}_2\| \le (\lambda_1 + \nu)X(t)^2, \tag{B.10}$$

$$|-\nu\boldsymbol{a}^\top\boldsymbol{w}_1 + \lambda_2\boldsymbol{a}^\top\boldsymbol{w}_2| \le \nu\|\boldsymbol{a}\|\|\boldsymbol{w}_1\| + \lambda_2\|\boldsymbol{a}\|\|\boldsymbol{w}_2\| \le (\nu + \lambda_2)X(t)^2, \tag{B.11}$$

$$\left|\sum_{i=3}^{d}\sigma^2(\boldsymbol{a}^\top\boldsymbol{w}_i)\right| \le \sum_{i=3}^{d}\sigma^2\|\boldsymbol{a}\|\|\boldsymbol{w}_i\| \le (d-2)\sigma^2X(t)^2. \tag{B.12}$$

Since $\operatorname{Tr}\boldsymbol{\Sigma} = \lambda_1 + \lambda_2 + (d-2)\sigma^2$ and $\nu = |\boldsymbol{v}_1^\top\boldsymbol{\Sigma}\boldsymbol{v}_2| \le \sqrt{\lambda_1\lambda_2} \le (\lambda_1 + \lambda_2)/2$, we have $(\lambda_1 + \nu) + (\nu + \lambda_2) + (d-2)\sigma^2 \le 2\operatorname{Tr}\boldsymbol{\Sigma}$.

Applying these bounds to Equations (9) to (12) lead to the following differential inequality for the time derivative of the maximum norm:

$$\tau\frac{d}{dt}X(t) \le \|\boldsymbol{\Sigma}_{xy}\|X(t) + 2\operatorname{Tr}\boldsymbol{\Sigma}X(t)^3. \tag{B.13}$$

Now we define $T_* := \frac{2\tau}{3(\|\boldsymbol{\Sigma}_{xy}\|+2\operatorname{Tr}\boldsymbol{\Sigma})}\log\frac{1}{s}$. Suppose for contradiction that $X(t) \geq 1$ for some $t \in [0, T_*)$. Since $X(0) = \bar{c}s < 1$ and $X(t)$ is continuous, there must exist a first time $T \in (0, T_*)$ such that $X(T) = 1$ and $X(t) < 1$ for all $t \in [0, T)$. Therefore, in this interval,

$$\tau\frac{d}{dt}X(t) \leq (\|\boldsymbol{\Sigma}_{xy}\| + 2\operatorname{Tr}\boldsymbol{\Sigma})X(t). \tag{B.14}$$

Integrating this inequality, we obtain

$$X(t) \leq X(0)e^{(\|\boldsymbol{\Sigma}_{xy}\|+2\operatorname{Tr}\boldsymbol{\Sigma})t/\tau}. \tag{B.15}$$

Since $T \leq T_*$ and $X(0) = \bar{c}s$, we have

$$X(T) \leq \bar{c}se^{(\|\boldsymbol{\Sigma}_{xy}\|+2\operatorname{Tr}\boldsymbol{\Sigma})T_*/\tau} = \bar{c}se^{2\log(1/s)/3} = \bar{c}s^{1/3}. \tag{B.16}$$

For all sufficiently small s, we have $\bar{c}s^{1/3} < 1/2$. This implies $X(T) \leq \bar{c}s^{1/3} < 1/2$. This contradicts $X(T) = 1$. Therefore, $X(t) < 1$ for all $t \in [0, T_*)$.

Consequently, Inequality (B.14) holds on $[0, T_*)$, and hence the desired bound Inequality (B.15) also follows. □

Proof of Lemma 3.1. By the definition of $X(t)$, we have

$$\|\boldsymbol{u}\| \leq \frac{1}{2}(\|\boldsymbol{a}\| + \|\boldsymbol{w}_1\|) \leq X(t), \quad \|\boldsymbol{v}\| \leq \frac{1}{2}(\|\boldsymbol{a}\| + \|\boldsymbol{w}_1\|) \leq X(t). \tag{B.17}$$

Therefore, we can uniformly bound the residual error terms (Equations (B.5) and (B.6)) similarly to the proof of Lemma B.1:

$$\|\boldsymbol{e}_u\| \leq 2\operatorname{Tr}\boldsymbol{\Sigma}X(t)^3, \quad \|\boldsymbol{e}_v\| \leq 2\operatorname{Tr}\boldsymbol{\Sigma}X(t)^3. \tag{B.18}$$

For $t < \frac{2\tau}{3(\|\boldsymbol{\Sigma}_{xy}\|+2\operatorname{Tr}\boldsymbol{\Sigma})}\log\frac{1}{s}$, Lemma B.1 implies

$$2\operatorname{Tr}\boldsymbol{\Sigma}X(t)^3 \leq C_{\text{res}}s^3e^{3(\|\boldsymbol{\Sigma}_{xy}\|+2\operatorname{Tr}\boldsymbol{\Sigma})t/\tau}, \tag{B.19}$$

where $C_{\text{res}} = 2\operatorname{Tr}\boldsymbol{\Sigma}\bar{c}^3$. Therefore,

$$\|\boldsymbol{e}_u\| \leq C_{\text{res}}s^3e^{3(\|\boldsymbol{\Sigma}_{xy}\|+2\operatorname{Tr}\boldsymbol{\Sigma})t/\tau}, \quad \|\boldsymbol{e}_v\| \leq C_{\text{res}}s^3e^{3(\|\boldsymbol{\Sigma}_{xy}\|+2\operatorname{Tr}\boldsymbol{\Sigma})t/\tau}. \tag{B.20}$$

Substituting the bound Inequality (B.20) into the integral terms (Equations (B.7) and (B.8)), we use the upper bound on t, which implies $s^3e^{3(\|\boldsymbol{\Sigma}_{xy}\|+2\operatorname{Tr}\boldsymbol{\Sigma})t/\tau} \leq s^3(s^{-2/3})^3 = s$. Therefore, for some constant $C_1 > 0$, we obtain

$$\begin{aligned}\left\|\frac{1}{\tau}\int_0^t e^{\|\boldsymbol{\Sigma}_{xy}\|(t-t')/\tau}\boldsymbol{e}_u(t')\,dt'\right\| &\leq \frac{1}{\tau}\int_0^t e^{\|\boldsymbol{\Sigma}_{xy}\|(t-t')/\tau}\,\|\boldsymbol{e}_u(t')\|\,dt' \\ &\leq \frac{C_{\text{res}}s^3}{\tau}e^{\|\boldsymbol{\Sigma}_{xy}\|t/\tau}\int_0^t e^{(3(\|\boldsymbol{\Sigma}_{xy}\|+2\operatorname{Tr}\boldsymbol{\Sigma})-\|\boldsymbol{\Sigma}_{xy}\|)t'/\tau}\,dt' \\ &\leq \frac{C_{\text{res}}s^3}{3(\|\boldsymbol{\Sigma}_{xy}\|+2\operatorname{Tr}\boldsymbol{\Sigma})-\|\boldsymbol{\Sigma}_{xy}\|}e^{3(\|\boldsymbol{\Sigma}_{xy}\|+2\operatorname{Tr}\boldsymbol{\Sigma})t/\tau} \\ &\leq C_1s,\end{aligned} \tag{B.21}$$

$$\begin{aligned}\left\|\frac{1}{\tau}\int_0^t e^{-\|\boldsymbol{\Sigma}_{xy}\|(t-t')/\tau}\boldsymbol{e}_v(t')\,dt'\right\| &\leq \frac{1}{\tau}\int_0^t e^{-\|\boldsymbol{\Sigma}_{xy}\|(t-t')/\tau}\,\|\boldsymbol{e}_v(t')\|\,dt' \\ &\leq \frac{C_{\text{res}}s^3}{\tau}e^{-\|\boldsymbol{\Sigma}_{xy}\|t/\tau}\int_0^t e^{(3(\|\boldsymbol{\Sigma}_{xy}\|+2\operatorname{Tr}\boldsymbol{\Sigma})+\|\boldsymbol{\Sigma}_{xy}\|)t'/\tau}\,dt' \\ &\leq \frac{C_{\text{res}}s^3}{3(\|\boldsymbol{\Sigma}_{xy}\|+2\operatorname{Tr}\boldsymbol{\Sigma})+\|\boldsymbol{\Sigma}_{xy}\|}e^{3(\|\boldsymbol{\Sigma}_{xy}\|+2\operatorname{Tr}\boldsymbol{\Sigma})t/\tau} \\ &\leq C_1s.\end{aligned} \tag{B.22}$$

By substituting the initial condition $\boldsymbol{u}(0) = \boldsymbol{r}_1$ and Inequality (B.21) into Equation (B.7), we get

$$\|\boldsymbol{u}(t) - \boldsymbol{r}_1 e^{\|\boldsymbol{\Sigma}_{xy}\| t/\tau}\| \leq C_1 s. \tag{B.23}$$

Likewise, applying Inequality (B.22) to Equation (B.8), we obtain

$$\|\boldsymbol{v}(t)\| \leq \|\boldsymbol{v}(0)\| e^{-\|\boldsymbol{\Sigma}_{xy}\| t/\tau} + C_1 s \leq C_2 s. \tag{B.24}$$

Finally, since $\boldsymbol{a} = \boldsymbol{u} + \boldsymbol{v}$ and $\boldsymbol{w}_1 = \boldsymbol{u} - \boldsymbol{v}$, applying the triangle inequality yields:

$$\|\boldsymbol{w}_1(t) - \boldsymbol{r}_1 e^{\|\boldsymbol{\Sigma}_{xy}\| t/\tau}\| \leq \|\boldsymbol{u}(t) - \boldsymbol{r}_1 e^{\|\boldsymbol{\Sigma}_{xy}\| t/\tau}\| + \|\boldsymbol{v}(t)\| \leq (C_1 + C_2)s, \tag{B.25}$$

$$\|\boldsymbol{a}(t) - \boldsymbol{r}_1 e^{\|\boldsymbol{\Sigma}_{xy}\| t/\tau}\| \leq \|\boldsymbol{u}(t) - \boldsymbol{r}_1 e^{\|\boldsymbol{\Sigma}_{xy}\| t/\tau}\| + \|\boldsymbol{v}(t)\| \leq (C_1 + C_2)s. \tag{B.26}$$

This proves the claim with $C = C_1 + C_2$.

□

B.2 Auxiliary Integral Bound

The following lemma will be used repeatedly in the next two subsections.

Lemma B.2. *Let $x(t) > 0$ satisfy $\tau \frac{d}{dt} x(t) \geq \gamma x(t)$ for some $\gamma > 0$. Let $M_K > 0$, $p > 0$, and $\beta \neq p\gamma$. If $K(t,t') \leq M_K e^{\beta(t-t')/\tau}$, then*

$$\frac{1}{\tau}\int_0^t K(t,t') x(t')^p \, dt' \leq M_K \begin{cases} \frac{x(t)^{\beta/\gamma} x(0)^{p-\beta/\gamma}}{\beta - \gamma p} & (\beta/\gamma > p), \\ \frac{x(t)^p}{\gamma p - \beta} & (0 < \beta/\gamma < p), \\ \frac{x(t)^p}{\gamma p} & (\beta \leq 0). \end{cases} . \tag{B.27}$$

Proof. After rescaling K, it suffices to treat the case $M_K = 1$. Since $\tau \frac{d}{dt} x \geq \gamma x$, we have $x(t) \geq x(t') e^{\gamma(t-t')/\tau}$ for $0 \leq t' \leq t$. Hence, for $\beta > 0$, $K(t,t') \leq e^{\beta(t-t')/\tau} \leq \left(\frac{x(t)}{x(t')}\right)^{\beta/\gamma}$. Using also $\tau \frac{d}{dt} x \geq \gamma x$,

$$\begin{aligned} \frac{1}{\tau}\int_0^t K(t,t') x(t')^p \, dt' &\leq \frac{1}{\gamma}\int_{x(0)}^{x(t)} \left(\frac{x(t)}{x}\right)^{\beta/\gamma} x^{p-1} \, dx \\ &\leq \frac{x(t)^{\beta/\gamma}}{\gamma}\int_{x(0)}^{x(t)} x^{p-1-\beta/\gamma} \, dx \\ &\leq \begin{cases} \frac{x(t)^{\beta/\gamma} x(0)^{p-\beta/\gamma}}{\beta - \gamma p} & (\beta/\gamma > p), \\ \frac{x(t)^p}{\gamma p - \beta} & (\beta/\gamma < p) \end{cases} \end{aligned} \tag{B.28}$$

If $\beta \leq 0$, then $K(t,t') \leq e^{\beta(t-t')/\tau} \leq 1$, so

$$\frac{1}{\tau}\int_0^t K(t,t') x(t')^p \, dt' \leq \frac{1}{\gamma}\int_{x(0)}^{x(t)} x^{p-1} \, dx \leq \frac{x(t)^p}{\gamma p}. \tag{B.29}$$

□

B.3 Global Boundedness of Orthogonal Components (Proof of Lemma 3.2)

This subsection establishes that the learning dynamics remain effectively confined to a low-dimensional subspace.

B.3.1 Preliminaries

We now establish the local bounds needed for the main argument, up to an exit time defined by the weight magnitudes.

Before analyzing the principal components, we briefly note the behavior of the weights $\boldsymbol{w}_i$ for $i \geq 3$. Taking the inner product with $\boldsymbol{w}_i$ on both sides of Equation (11) yields $\tau \frac{d}{dt}\|\boldsymbol{w}_i\|^2 \leq -2\sigma^2(\boldsymbol{a}^\top \boldsymbol{w}_i)^2 \leq 0$. Given the initialization $\|\boldsymbol{w}_i(0)\| \leq \bar{c}s$, it immediately follows that $\|\boldsymbol{w}_i(t)\| \leq \bar{c}s$ for all $t > 0$. Therefore, we focus on the remaining components.

Before proceeding to the main local analysis up to the exit time, we examine the behavior of $\boldsymbol{u}$ and $\boldsymbol{v}$ in the earliest stage of learning. Lemma B.3 establishes that $\boldsymbol{u}$ eventually surpasses $\boldsymbol{v}$ regardless of the relative magnitudes of the initial weights.

Lemma B.3. *For all sufficiently small $s > 0$, if $t^* = \frac{\tau}{2\|\boldsymbol{\Sigma}_{xy}\|} \log\left(\frac{c_{v0}}{c_{u0}} + 2\right)$, then the following inequality holds:*

$$\|\boldsymbol{v}(t^*)\| \leq \|\boldsymbol{u}(t^*)\|. \tag{B.30}$$

Proof. Since t^* is independent of s, we have

$$t^* < \frac{2\tau}{3(\|\boldsymbol{\Sigma}_{xy}\| + 2\operatorname{Tr}\boldsymbol{\Sigma})} \log\frac{1}{s} \tag{B.31}$$

for all sufficiently small s. Applying the bound from Lemma B.1 on the interval $[0, t^*]$, we obtain

$$X(t) \leq X(0)e^{(\|\boldsymbol{\Sigma}_{xy}\| + 2\operatorname{Tr}\boldsymbol{\Sigma})t/\tau} \leq C_X s, \tag{B.32}$$

for some constant $C_X > 0$. Because the residuals $\boldsymbol{e}_u(t)$ and $\boldsymbol{e}_v(t)$ scale as $X(t)^3$, this guarantees that their corresponding integral terms are uniformly bounded by $O(s^3)$. Specifically, there exists a constant $C_* > 0$ such that the integral bounds satisfy:

$$\left\| \int_0^{t^*} e^{\|\boldsymbol{\Sigma}_{xy}\|(t^*-t')/\tau} \boldsymbol{e}_u(t')\, dt' \right\|, \ \left\| \int_0^{t^*} e^{-\|\boldsymbol{\Sigma}_{xy}\|(t^*-t')/\tau} \boldsymbol{e}_v(t')\, dt' \right\| \leq C_* s^3. \tag{B.33}$$

Using Equations (B.7) and (B.8), we get

$$\|\boldsymbol{u}(t^*)\| \geq e^{\|\boldsymbol{\Sigma}_{xy}\|t^*/\tau}\|\boldsymbol{u}(0)\| - C_* s^3, \tag{B.34}$$

$$\|\boldsymbol{v}(t^*)\| \leq e^{-\|\boldsymbol{\Sigma}_{xy}\|t^*/\tau}\|\boldsymbol{v}(0)\| + C_* s^3. \tag{B.35}$$

Since

$$e^{\|\boldsymbol{\Sigma}_{xy}\|t^*/\tau} = \sqrt{\frac{c_{v0}}{c_{u0}} + 2}, \qquad e^{-\|\boldsymbol{\Sigma}_{xy}\|t^*/\tau} = \frac{1}{\sqrt{\frac{c_{v0}}{c_{u0}} + 2}}, \tag{B.36}$$

and $\|\boldsymbol{u}(0)\| = c_{u0}s$, $\|\boldsymbol{v}(0)\| = c_{v0}s$, we obtain

$$\begin{aligned} \|\boldsymbol{u}(t^*)\| - \|\boldsymbol{v}(t^*)\| &\geq \left(c_{u0}\sqrt{\frac{c_{v0}}{c_{u0}} + 2} - \frac{c_{v0}}{\sqrt{\frac{c_{v0}}{c_{u0}} + 2}} \right) s - 2C_* s^3 \\ &= \frac{2c_{u0}}{\sqrt{\frac{c_{v0}}{c_{u0}} + 2}} s - 2C_* s^3. \end{aligned} \tag{B.37}$$

The coefficient of s is strictly positive, so for sufficiently small s the $O(s)$ term dominates the $O(s^3)$ remainder. Hence $\|\boldsymbol{u}(t^*)\| \geq \|\boldsymbol{v}(t^*)\|$. □

The preceding analysis shows that the network parameters remain of order $O(s)$ during this very early phase of learning. Furthermore, Lemma B.3 ensures that even if the initial weights satisfy $\|\boldsymbol{v}(0)\| > \|\boldsymbol{u}(0)\|$, there exists a time t^* at which $\|\boldsymbol{u}(t^*)\| \geq \|\boldsymbol{v}(t^*)\|$, while all weights are still bounded by $O(s)$. Therefore, we may assume $\|\boldsymbol{v}(0)\| \leq \|\boldsymbol{u}(0)\|$ without loss of generality. (Note that, since t^* is independent of s and all weights remain $O(s)$ on $[0, t^*]$, this contribution of dynamics up to t_* can be absorbed into the constants of the subsequent bounds.)

To rigorously evaluate the dynamics before the weights grow to an $O(1)$ scale, we introduce an exit time T_ε as the first time the maximum norm of the weights reaches a predefined threshold ε:

$$T_\varepsilon := \inf\{t > 0 : \max\{\|\boldsymbol{a}(t)\|, \|\boldsymbol{w}_1(t)\|, \|\boldsymbol{w}_2(t)\|, \ldots, \|\boldsymbol{w}_d(t)\|\} \geq \varepsilon\} \tag{B.38}$$

where $\varepsilon > 0$ is a constant independent of the initialization scale s. The exact value of ε will be chosen to be sufficiently small to ensure that the following propositions hold throughout the interval $[0, T_\varepsilon]$.

Lemma B.4. *There exists a constant $c_1 > 0$ such that for all $t \in [0, T_\varepsilon]$, the following inequalities hold:*

$$\|\boldsymbol{v}(t)\| \leq \|\boldsymbol{u}(t)\|, \tag{B.39}$$

$$\tau \frac{d}{dt}\|\boldsymbol{u}(t)\| \geq c_1 \|\boldsymbol{u}(t)\|. \tag{B.40}$$

Consequently, for any times t' and t satisfying $0 \leq t' \leq t \leq T_\varepsilon$, we have

$$\|\boldsymbol{u}(t')\| \leq \|\boldsymbol{u}(t)\| e^{-c_1(t-t')/\tau}. \tag{B.41}$$

Proof. Since $\|\boldsymbol{a}\| \leq \|\boldsymbol{u}\| + \|\boldsymbol{v}\|$, the definition of T_ε (Equation (B.38)) gives, for all $t \in [0, T_\varepsilon]$,

$$|\lambda_1 \boldsymbol{a}^\top \boldsymbol{w}_1 - \nu \boldsymbol{a}^\top \boldsymbol{w}_2| \leq \lambda_1 \|\boldsymbol{a}\|\|\boldsymbol{w}_1\| + \nu\|\boldsymbol{a}\|\|\boldsymbol{w}_2\| \leq (\lambda_1 + \nu)\varepsilon(\|\boldsymbol{u}\| + \|\boldsymbol{v}\|), \tag{B.42}$$

$$|-\nu \boldsymbol{a}^\top \boldsymbol{w}_1 + \lambda_2 \boldsymbol{a}^\top \boldsymbol{w}_2| \leq \nu\|\boldsymbol{a}\|\|\boldsymbol{w}_1\| + \lambda_2\|\boldsymbol{a}\|\|\boldsymbol{w}_2\| \leq (\nu + \lambda_2)\varepsilon(\|\boldsymbol{u}\| + \|\boldsymbol{v}\|), \tag{B.43}$$

$$\left|\sum_{i=3}^{d} \sigma^2(\boldsymbol{a}^\top \boldsymbol{w}_i)\right| \leq \sum_{i=3}^{d} \sigma^2 \|\boldsymbol{a}\|\|\boldsymbol{w}_i\| \leq (d-2)\sigma^2\varepsilon(\|\boldsymbol{u}\| + \|\boldsymbol{v}\|). \tag{B.44}$$

Hence there exists $C_0 > 0$ such that the residual terms $\boldsymbol{e}_u$ and $\boldsymbol{e}_v$ (Equations (B.5) and (B.6)) satisfy

$$\|\boldsymbol{e}_u\|, \|\boldsymbol{e}_v\| \leq \frac{1}{2} C_0 \varepsilon^2 (\|\boldsymbol{u}\| + \|\boldsymbol{v}\|). \tag{B.45}$$

Applying these to Equations (B.3) and (B.4) yields

$$\tau \frac{d}{dt}\|\boldsymbol{u}\| \geq \|\boldsymbol{\Sigma}_{xy}\|\|\boldsymbol{u}\| - \frac{1}{2} C_0 \varepsilon^2 (\|\boldsymbol{u}\| + \|\boldsymbol{v}\|), \tag{B.46}$$

$$\tau \frac{d}{dt}\|\boldsymbol{v}\| \leq -\|\boldsymbol{\Sigma}_{xy}\|\|\boldsymbol{v}\| + \frac{1}{2} C_0 \varepsilon^2 (\|\boldsymbol{u}\| + \|\boldsymbol{v}\|). \tag{B.47}$$

Subtracting the second inequality from the first,

$$\tau \frac{d}{dt}(\|\boldsymbol{u}\| - \|\boldsymbol{v}\|) \geq (\|\boldsymbol{\Sigma}_{xy}\| - C_0\varepsilon^2)(\|\boldsymbol{u}\| + \|\boldsymbol{v}\|). \tag{B.48}$$

Choosing ε sufficiently small so that $\|\boldsymbol{\Sigma}_{xy}\| - C_0\varepsilon^2 \geq 0$, we obtain $\tau \frac{d}{dt}(\|\boldsymbol{u}\| - \|\boldsymbol{v}\|) \geq 0$ on $[0, T_\varepsilon]$. Since $\|\boldsymbol{u}(0)\| \geq \|\boldsymbol{v}(0)\|$, it follows that $\|\boldsymbol{u}(t)\| \geq \|\boldsymbol{v}(t)\|$ for all $t \in [0, T_\varepsilon]$.

Also, from Inequality (B.46),

$$\begin{aligned} \tau \frac{d}{dt}\|\boldsymbol{u}\| &\geq \|\boldsymbol{\Sigma}_{xy}\|\|\boldsymbol{u}\| - \frac{1}{2} C_0 \varepsilon^2 (\|\boldsymbol{u}\| + \|\boldsymbol{v}\|) \\ &\geq (\|\boldsymbol{\Sigma}_{xy}\| - C_0\varepsilon^2)\|\boldsymbol{u}\|. \end{aligned} \tag{B.49}$$

Setting

$$c_1 := \|\boldsymbol{\Sigma}_{xy}\| - C_0\varepsilon^2 \tag{B.50}$$

and taking ε smaller if necessary, we can ensure $c_1 > 0$, which gives Inequality (B.40):

$$\tau\frac{d}{dt}\|\boldsymbol{u}(t)\| \geq c_1\|\boldsymbol{u}(t)\|. \tag{B.51}$$

Integrating from t' to t yields

$$\ln\left(\frac{\|\boldsymbol{u}(t)\|}{\|\boldsymbol{u}(t')\|}\right) \geq \frac{c_1}{\tau}(t-t'). \tag{B.52}$$

Rearranging gives Inequality (B.41):

$$\|\boldsymbol{u}(t')\| \leq \|\boldsymbol{u}(t)\|e^{-c_1(t-t')/\tau}. \tag{B.53}$$

□

Lemma B.5. *There exist constants $C_{w_2 1}, C_{w_2 2} > 0$ such that for all $t \in [0, T_\varepsilon]$, the following inequality holds:*

$$\|\boldsymbol{w}_2(t)\| \leq C_{w_2 1}s + C_{w_2 2}\|\boldsymbol{u}(t)\|^3. \tag{B.54}$$

Proof. Using $|\boldsymbol{a}^\top\boldsymbol{w}_1| \leq \|\boldsymbol{u}\|^2$, $\|\boldsymbol{a}\| \leq 2\|\boldsymbol{u}\|$, and $|\boldsymbol{a}^\top\boldsymbol{w}_2| \leq 2\|\boldsymbol{u}\|\|\boldsymbol{w}_2\|$ in Equation (10), we obtain

$$\tau\frac{d}{dt}\|\boldsymbol{w}_2\| \leq 4\lambda_2\|\boldsymbol{u}\|^2\|\boldsymbol{w}_2\| + 2\nu\|\boldsymbol{u}\|^3. \tag{B.55}$$

Let

$$K(t,t') := \exp\left(\frac{1}{\tau}\int_{t'}^{t} 4\lambda_2\|\boldsymbol{u}(r)\|^2\, dr\right). \tag{B.56}$$

The variation of constants formula gives:

$$\|\boldsymbol{w}_2(t)\| \leq K(t,0)\|\boldsymbol{w}_2(0)\| + \frac{2\nu}{\tau}\int_0^t K(t,t')\|\boldsymbol{u}(t')\|^3\, dt'. \tag{B.57}$$

By Inequality (B.41) and $\|\boldsymbol{u}(t)\| \leq \varepsilon$, for $0 \leq t' \leq t \leq T_\varepsilon$,

$$\frac{1}{\tau}\int_{t'}^{t} 4\lambda_2\|\boldsymbol{u}(r)\|^2\, dr \leq \frac{4\lambda_2\|\boldsymbol{u}(t)\|^2}{\tau}\int_{t'}^{t} e^{-2c_1(t-r)/\tau}\, dr \leq \frac{2\lambda_2}{c_1}\varepsilon^2. \tag{B.58}$$

Hence $K(t,t') \leq e^{\frac{2\lambda_2}{c_1}\varepsilon^2} =: C_K$. Applying Lemma B.2 with $x(t) = \|\boldsymbol{u}(t)\|$, $\gamma = c_1$, $\beta = 0$, and $p = 3$, we obtain

$$\frac{1}{\tau}\int_0^t K(t,t')\|\boldsymbol{u}(t')\|^3\, dt' \leq \frac{C_K}{3c_1}\|\boldsymbol{u}(t)\|^3. \tag{B.59}$$

Substituting this into Inequality (B.57) yields:

$$\begin{aligned}\|\boldsymbol{w}_2(t)\| &\leq C_K\|\boldsymbol{w}_2(0)\| + \frac{2\nu C_K}{3c_1}\|\boldsymbol{u}(t)\|^3 \\ &\leq C_{w_2 1}s + C_{w_2 2}\|\boldsymbol{u}(t)\|^3\end{aligned} \tag{B.60}$$

for some constants $C_{w_2 1}, C_{w_2 2} > 0$. □

Corollary B.6. *There exists a constant $C_u > 0$ such that for all $t \in [0, T_\varepsilon]$,*

$$\|\boldsymbol{v}(t)\|, \|\boldsymbol{a}(t)\|, \|\boldsymbol{w}_i(t)\| \leq C_u\|\boldsymbol{u}(t)\|, \qquad (i = 1, \ldots, d). \tag{B.61}$$

Proof. By Inequalities (B.39) and (B.40), we have $\|\boldsymbol{v}(t)\| \le \|\boldsymbol{u}(t)\|$ and $\|\boldsymbol{u}(t)\| \ge \|\boldsymbol{u}(0)\| = c_{u0}s$ on $[0, T_\varepsilon]$. Hence

$$\|\boldsymbol{a}(t)\| = \|\boldsymbol{u}(t) + \boldsymbol{v}(t)\| \le 2\|\boldsymbol{u}(t)\|, \quad \|\boldsymbol{w}_1(t)\| = \|\boldsymbol{u}(t) - \boldsymbol{v}(t)\| \le 2\|\boldsymbol{u}(t)\|. \tag{B.62}$$

Moreover, Lemma B.5 and $\|\boldsymbol{u}(t)\| \le \varepsilon$ yield

$$\|\boldsymbol{w}_2(t)\| \le C_{w_21}s + C_{w_22}\|\boldsymbol{u}(t)\|^3 \le \left(\frac{C_{w_21}}{c_{u0}} + C_{w_22}\varepsilon^2\right)\|\boldsymbol{u}(t)\|. \tag{B.63}$$

For $i \ge 3$, the monotonicity argument from the beginning of this subsection gives

$$\|\boldsymbol{w}_i(t)\| \le \bar{c}s \le \frac{\bar{c}}{c_{u0}}\|\boldsymbol{u}(t)\|. \tag{B.64}$$

The claim follows by taking C_u to be the maximum of the constants above. □

B.3.2 Main Proof of Lemma 3.2

Proof of Lemma 3.2. We aim to show that the vector $\boldsymbol{e}_\perp := ((\boldsymbol{P}_\perp\boldsymbol{u})^\top, (\boldsymbol{P}_\perp\boldsymbol{v})^\top, (\boldsymbol{P}_\perp\boldsymbol{w}_2)^\top, \dots, (\boldsymbol{P}_\perp\boldsymbol{w}_d)^\top)^\top \in \mathbb{R}^{m(d+1)}$, which captures all components of the system orthogonal to the condensation direction $\hat{\boldsymbol{r}}_1$, remains $O(s)$ uniformly in time. Since $\boldsymbol{a} = \boldsymbol{u} + \boldsymbol{v}$ and $\boldsymbol{w}_1 = \boldsymbol{u} - \boldsymbol{v}$, controlling $\boldsymbol{P}_\perp\boldsymbol{u}$ and $\boldsymbol{P}_\perp\boldsymbol{v}$ is equivalent to controlling the orthogonal parts of both $\boldsymbol{a}$ and $\boldsymbol{w}_1$.

We introduce $\boldsymbol{\theta}(t) := \boldsymbol{W}(t)^\top\boldsymbol{a}(t)$ and $r_i(t) := \boldsymbol{v}_i^\top\boldsymbol{\Sigma}(\boldsymbol{\beta} - \boldsymbol{\theta}(t))$. Since $\boldsymbol{\Sigma\beta} = \boldsymbol{\Sigma}_{xy} = \|\boldsymbol{\Sigma}_{xy}\|\boldsymbol{v}_1$,

$$\boldsymbol{\Sigma v}_1 = \lambda_1\boldsymbol{v}_1 - \nu\boldsymbol{v}_2, \quad \boldsymbol{\Sigma v}_2 = -\nu\boldsymbol{v}_1 + \lambda_2\boldsymbol{v}_2, \quad \boldsymbol{\Sigma v}_i = \sigma^2\boldsymbol{v}_i \ \ (i \ge 3), \tag{B.65}$$

and $\boldsymbol{\theta}(t) = \sum_{j=1}^d(\boldsymbol{a}^\top\boldsymbol{w}_j)\boldsymbol{v}_j$, we obtain

$$r_1(t) = \|\boldsymbol{\Sigma}_{xy}\| - \lambda_1\boldsymbol{a}^\top\boldsymbol{w}_1 + \nu\boldsymbol{a}^\top\boldsymbol{w}_2, \quad r_2(t) = \nu\boldsymbol{a}^\top\boldsymbol{w}_1 - \lambda_2\boldsymbol{a}^\top\boldsymbol{w}_2, \quad r_i(t) = -\sigma^2\boldsymbol{a}^\top\boldsymbol{w}_i \ \ (i = 3, \dots, d). \tag{B.66}$$

In terms of these scalar coefficients, Equations (10), (11), (B.3) and (B.4) become

$$\tau\frac{d}{dt}\boldsymbol{u} = r_1\boldsymbol{u} + \frac{r_2}{2}\boldsymbol{w}_2 + \frac{1}{2}\sum_{i=3}^d r_i\boldsymbol{w}_i, \tag{B.67}$$

$$\tau\frac{d}{dt}\boldsymbol{v} = -r_1\boldsymbol{v} + \frac{r_2}{2}\boldsymbol{w}_2 + \frac{1}{2}\sum_{i=3}^d r_i\boldsymbol{w}_i, \tag{B.68}$$

$$\tau\frac{d}{dt}\boldsymbol{w}_i = r_i(\boldsymbol{u} + \boldsymbol{v}), \qquad (i = 2, \dots, d). \tag{B.69}$$

Applying the projection operator $\boldsymbol{P}_\perp$ to these equations preserves the same scalar coefficients, so the orthogonal components satisfy

$$\tau\frac{d}{dt}\boldsymbol{P}_\perp\boldsymbol{u} = r_1\boldsymbol{P}_\perp\boldsymbol{u} + \frac{r_2}{2}\boldsymbol{P}_\perp\boldsymbol{w}_2 + \frac{1}{2}\sum_{i=3}^d r_i\boldsymbol{P}_\perp\boldsymbol{w}_i, \tag{B.70}$$

$$\tau\frac{d}{dt}\boldsymbol{P}_\perp\boldsymbol{v} = -r_1\boldsymbol{P}_\perp\boldsymbol{v} + \frac{r_2}{2}\boldsymbol{P}_\perp\boldsymbol{w}_2 + \frac{1}{2}\sum_{i=3}^d r_i\boldsymbol{P}_\perp\boldsymbol{w}_i, \tag{B.71}$$

$$\tau\frac{d}{dt}\boldsymbol{P}_\perp\boldsymbol{w}_i = r_i(\boldsymbol{P}_\perp\boldsymbol{u} + \boldsymbol{P}_\perp\boldsymbol{v}), \qquad (i = 2, \dots, d). \tag{B.72}$$

Stacking the above equations yields

$$\tau\frac{d}{dt}\boldsymbol{e}_\perp = \boldsymbol{R}\boldsymbol{e}_\perp, \tag{B.73}$$

where

$$\boldsymbol{R}(t) = \begin{pmatrix} r_1(t) & 0 & \frac{r_2(t)}{2} & \frac{r_3(t)}{2} & \dots & \frac{r_d(t)}{2} \\ 0 & -r_1(t) & \frac{r_2(t)}{2} & \frac{r_3(t)}{2} & \dots & \frac{r_d(t)}{2} \\ r_2(t) & r_2(t) & 0 & 0 & \dots & 0 \\ r_3(t) & r_3(t) & 0 & 0 & \dots & 0 \\ \vdots & \vdots & \vdots & \vdots & \ddots & \vdots \\ r_d(t) & r_d(t) & 0 & 0 & \dots & 0 \end{pmatrix} \otimes \boldsymbol{I}_m. \tag{B.74}$$

The proof proceeds in two steps: we first bound the dynamics up to the predefined exit time T_ε, and then bound the subsequent evolution on the interval $[T_\varepsilon, \infty)$.

Step 1: Bounding the dynamics up to T_ε. Let $\widetilde{\boldsymbol{\Lambda}} := \operatorname{diag}(\|\boldsymbol{\Sigma}_{xy}\|, -\|\boldsymbol{\Sigma}_{xy}\|, 0, \dots, 0) \otimes \boldsymbol{I}_m$, so that

$$\tau \frac{d}{dt} \boldsymbol{e}_\perp = (\widetilde{\boldsymbol{\Lambda}} + (\boldsymbol{R} - \widetilde{\boldsymbol{\Lambda}}))\boldsymbol{e}_\perp. \tag{B.75}$$

On $[0, T_\varepsilon]$, Corollary B.6 yields $\|\boldsymbol{a}(t)\|, \|\boldsymbol{w}_i(t)\| \leq C_u \|\boldsymbol{u}(t)\|$ for every $i = 1, \dots, d$. Therefore each product appearing in the coefficients $r_1 - \|\boldsymbol{\Sigma}_{xy}\|$, r_2, and r_i is of the form $\boldsymbol{a}^\top \boldsymbol{w}_j$ and is bounded by

$$|\boldsymbol{a}^\top \boldsymbol{w}_j| \leq \|\boldsymbol{a}\| \|\boldsymbol{w}_j\| \leq C_u^2 \|\boldsymbol{u}\|^2, \qquad (j = 1, \dots, d). \tag{B.76}$$

From the definitions of Equations (B.66) and (B.74), it follows that there exists a constant $C_{R1} > 0$ such that, for all $t \in [0, T_\varepsilon]$,

$$\|\boldsymbol{R}(t) - \widetilde{\boldsymbol{\Lambda}}\| \leq C_{R1} \|\boldsymbol{u}(t)\|^2. \tag{B.77}$$

Define the running supremum $\overline{e}_\perp(t) := \sup_{t' \in [0,t]} \|\boldsymbol{e}_\perp(t')\|$. Applying the variation of constants formula gives

$$\boldsymbol{e}_\perp(t) = e^{\widetilde{\boldsymbol{\Lambda}} t/\tau} \boldsymbol{e}_\perp(0) + \frac{1}{\tau} \int_0^t e^{\widetilde{\boldsymbol{\Lambda}}(t-t')/\tau} (\boldsymbol{R}(t') - \widetilde{\boldsymbol{\Lambda}}) \boldsymbol{e}_\perp(t')\, dt'. \tag{B.78}$$

For the first term, since $\boldsymbol{P}_\perp \boldsymbol{u}(0) = 0$,

$$e^{\widetilde{\boldsymbol{\Lambda}} t/\tau} \boldsymbol{e}_\perp(0) = (0, e^{-\|\boldsymbol{\Sigma}_{xy}\| t/\tau} \boldsymbol{P}_\perp \boldsymbol{v}(0), \boldsymbol{P}_\perp \boldsymbol{w}_2(0), \dots, \boldsymbol{P}_\perp \boldsymbol{w}_d(0))^\top \tag{B.79}$$

and hence

$$\|e^{\widetilde{\boldsymbol{\Lambda}} t/\tau} \boldsymbol{e}_\perp(0)\| \leq C_{e1} s. \tag{B.80}$$

For the second term, we use $\|e^{\widetilde{\boldsymbol{\Lambda}}(t-t')/\tau}\| \leq e^{\|\boldsymbol{\Sigma}_{xy}\|(t-t')/\tau}$ and Inequality (B.77):

$$\begin{aligned} \left\| \frac{1}{\tau} \int_0^t e^{\widetilde{\boldsymbol{\Lambda}}(t-t')/\tau} (\boldsymbol{R}(t') - \widetilde{\boldsymbol{\Lambda}}) \boldsymbol{e}_\perp(t')\, dt' \right\| &\leq \frac{1}{\tau} \int_0^t \|e^{\widetilde{\boldsymbol{\Lambda}}(t-t')/\tau}\| \|\boldsymbol{R}(t') - \widetilde{\boldsymbol{\Lambda}}\| \|\boldsymbol{e}_\perp(t')\|\, dt' \\ &\leq C_{R1} \overline{e}_\perp(t) \frac{1}{\tau} \int_0^t e^{\|\boldsymbol{\Sigma}_{xy}\|(t-t')/\tau} \|\boldsymbol{u}(t')\|^2\, dt'. \end{aligned} \tag{B.81}$$

Apply Lemma B.2 with $x(t) = \|\boldsymbol{u}(t)\|$, $\gamma = c_1$, $\beta = \|\boldsymbol{\Sigma}_{xy}\|$, and $p = 2$. By Inequality (B.40), $\tau \frac{d}{dt} x(t) \geq c_1 x(t)$, and since $c_1 = \|\boldsymbol{\Sigma}_{xy}\| - C_0 \varepsilon^2$, choosing ε sufficiently small ensures $\beta/\gamma = \|\boldsymbol{\Sigma}_{xy}\|/c_1 \in (1, 2)$. Thus the second case of Lemma B.2 yields

$$\frac{1}{\tau} \int_0^t e^{\|\boldsymbol{\Sigma}_{xy}\|(t-t')/\tau} \|\boldsymbol{u}(t')\|^2\, dt' \leq \frac{\|\boldsymbol{u}(t)\|^2}{2c_1 - \|\boldsymbol{\Sigma}_{xy}\|} \leq \frac{\varepsilon^2}{\|\boldsymbol{\Sigma}_{xy}\| - 2C_0 \varepsilon^2}. \tag{B.82}$$

Combining the above estimates, we arrive at

$$\overline{e}_\perp(t) \leq C_{e1} s + \frac{C_{R1} \varepsilon^2}{\|\boldsymbol{\Sigma}_{xy}\| - 2C_0 \varepsilon^2} \overline{e}_\perp(t). \tag{B.83}$$

Taking ε smaller if necessary so that $\frac{C_{R1}\varepsilon^2}{\|\boldsymbol{\Sigma}_{xy}\| - 2C_0\varepsilon^2} \leq \frac{1}{2}$, we obtain

$$\sup_{t \in [0, T_\varepsilon]} \|\boldsymbol{e}_\perp(t)\| = \overline{e}_\perp(T_\varepsilon) \leq 2C_{e1} s. \tag{B.84}$$

Step 2: Bounding the dynamics over the infinite horizon $[T_\varepsilon, \infty)$. Consider the loss

$$\mathcal{L}(t) = (\boldsymbol{\theta}(t) - \boldsymbol{\beta})^\top \boldsymbol{\Sigma}(\boldsymbol{\theta}(t) - \boldsymbol{\beta}) = \boldsymbol{\beta}^\top \boldsymbol{\Sigma}\boldsymbol{\beta} - 2\boldsymbol{\beta}^\top \boldsymbol{\Sigma}\boldsymbol{\theta}(t) + \boldsymbol{\theta}(t)^\top \boldsymbol{\Sigma}\boldsymbol{\theta}(t). \tag{B.85}$$

Under the gradient flow,

$$\tau \frac{d\mathcal{L}}{dt} = \nabla_{\boldsymbol{a}} \mathcal{L}^\top \frac{d\boldsymbol{a}}{dt} + \sum_{i=1}^{d} \nabla_{\boldsymbol{w}_i} \mathcal{L}^\top \frac{d\boldsymbol{w}_i}{dt} = -\|\nabla_{\boldsymbol{a},\boldsymbol{W}} \mathcal{L}\|^2 \leq 0. \tag{B.86}$$

Since $\boldsymbol{\theta} = \boldsymbol{W}^\top \boldsymbol{a}$, the chain rule gives $\nabla_{\boldsymbol{W}} \mathcal{L} = \boldsymbol{a}(\nabla_{\boldsymbol{\theta}} \mathcal{L})^\top$ and hence $\|\nabla_{\boldsymbol{W}} \mathcal{L}\|_F^2 = \|\boldsymbol{a}\|^2 \|\nabla_{\boldsymbol{\theta}} \mathcal{L}\|^2$. Thus,

$$\|\nabla_{\boldsymbol{a},\boldsymbol{W}} \mathcal{L}\|^2 = \|\nabla_{\boldsymbol{a}} \mathcal{L}\|^2 + \|\nabla_{\boldsymbol{W}} \mathcal{L}\|_F^2 = \|\nabla_{\boldsymbol{a}} \mathcal{L}\|^2 + \|\boldsymbol{a}\|^2 \|\nabla_{\boldsymbol{\theta}} \mathcal{L}\|^2 \geq \|\boldsymbol{a}\|^2 \|\nabla_{\boldsymbol{\theta}} \mathcal{L}\|^2, \tag{B.87}$$

$$\|\nabla_{\boldsymbol{\theta}} \mathcal{L}\|^2 = 4\|\boldsymbol{\Sigma}(\boldsymbol{\theta} - \boldsymbol{\beta})\|^2 \geq 4\sigma^2 (\boldsymbol{\theta} - \boldsymbol{\beta})^\top \boldsymbol{\Sigma}(\boldsymbol{\theta} - \boldsymbol{\beta}) = 4\sigma^2 \mathcal{L}(t). \tag{B.88}$$

By Lemma B.5, choosing ε sufficiently small and then s sufficiently small gives $\|\boldsymbol{w}_2(t)\| \leq \varepsilon/2$ for $t \leq T_\varepsilon$, while $\|\boldsymbol{w}_i(t)\| \leq \bar{c}s \leq \varepsilon/2$ for $i \geq 3$. Hence the exit at time T_ε must occur through $\boldsymbol{a}$ or $\boldsymbol{w}_1$, so

$$\|\boldsymbol{u}(T_\varepsilon)\| + \|\boldsymbol{v}(T_\varepsilon)\| \geq \max\{\|\boldsymbol{a}(T_\varepsilon)\|, \|\boldsymbol{w}_1(T_\varepsilon)\|\} = \varepsilon. \tag{B.89}$$

Also, using the same variation of constants argument as in the proof of Lemma B.5, we obtain

$$\|\boldsymbol{v}(T_\varepsilon)\| \leq \|\boldsymbol{v}(0)\| + \frac{C_0 \varepsilon^2}{c_1} \|\boldsymbol{u}(T_\varepsilon)\|. \tag{B.90}$$

Since $\|\boldsymbol{v}(0)\| = O(s)$, taking ε small enough that $C_0\varepsilon^2/c_1 \leq 1/3$, and then s small enough, this yields $\|\boldsymbol{v}(T_\varepsilon)\| \leq \|\boldsymbol{u}(T_\varepsilon)\|/3 + O(s)$, hence $\boldsymbol{a}(T_\varepsilon)^\top \boldsymbol{w}_1(T_\varepsilon) = \|\boldsymbol{u}(T_\varepsilon)\|^2 - \|\boldsymbol{v}(T_\varepsilon)\|^2 \geq \varepsilon^2/4$.

Since all weight norms are at most ε at time T_ε, we have $\|\boldsymbol{\theta}(T_\varepsilon)\| = O(\varepsilon^2)$ and therefore $\boldsymbol{\theta}(T_\varepsilon)^\top \boldsymbol{\Sigma}\boldsymbol{\theta}(T_\varepsilon) = O(\varepsilon^4)$. On the other hand, $\boldsymbol{\beta}^\top \boldsymbol{\Sigma}\boldsymbol{\theta}(T_\varepsilon) = \boldsymbol{\Sigma}_{xy}^\top \boldsymbol{\theta}(T_\varepsilon) = \|\boldsymbol{\Sigma}_{xy}\| \boldsymbol{a}(T_\varepsilon)^\top \boldsymbol{w}_1(T_\varepsilon) \geq \|\boldsymbol{\Sigma}_{xy}\|\varepsilon^2/4$. Hence there exists $c_{\mathcal{L}} > 0$, independent of s, such that

$$\mathcal{L}(T_\varepsilon) \leq \boldsymbol{\beta}^\top \boldsymbol{\Sigma}\boldsymbol{\beta} - 2 \cdot \frac{\|\boldsymbol{\Sigma}_{xy}\|}{4}\varepsilon^2 + O(\varepsilon^4) \leq \boldsymbol{\beta}^\top \boldsymbol{\Sigma}\boldsymbol{\beta} - c_{\mathcal{L}}\varepsilon^2. \tag{B.91}$$

For any $t \geq T_\varepsilon$, Equation (B.86) gives $\mathcal{L}(t) \leq \mathcal{L}(T_\varepsilon)$, while $\mathcal{L}(t) \geq \boldsymbol{\beta}^\top \boldsymbol{\Sigma}\boldsymbol{\beta} - 2\boldsymbol{\beta}^\top \boldsymbol{\Sigma}\boldsymbol{\theta}(t) \geq \boldsymbol{\beta}^\top \boldsymbol{\Sigma}\boldsymbol{\beta} - 2\|\boldsymbol{\Sigma}_{xy}\|\|\boldsymbol{\theta}(t)\|$. Therefore $\|\boldsymbol{\theta}(t)\| \geq \frac{c_{\mathcal{L}}}{2\|\boldsymbol{\Sigma}_{xy}\|}\varepsilon^2 =: C_\theta$ for all $t \geq T_\varepsilon$.

Let $\boldsymbol{M} := \boldsymbol{a}\boldsymbol{a}^\top - \boldsymbol{W}\boldsymbol{W}^\top$, which is the conserved quantity and satisfies $\|\boldsymbol{M}\| = O(s^2)$. Since $\|\boldsymbol{\theta}(t)\|^2 = \boldsymbol{a}(t)^\top \boldsymbol{W}(t)\boldsymbol{W}(t)^\top \boldsymbol{a}(t) = \|\boldsymbol{a}(t)\|^4 - \boldsymbol{a}(t)^\top \boldsymbol{M}\boldsymbol{a}(t)$, we get $\|\boldsymbol{a}(t)\|^4 - C_\theta^2 \geq -\|\boldsymbol{M}\|\|\boldsymbol{a}(t)\|^2$, hence $\|\boldsymbol{a}(t)\|^2 \geq C_\theta - \|\boldsymbol{M}\|/2$. For all sufficiently small s, this yields $\|\boldsymbol{a}(t)\| \geq \sqrt{C_\theta/2} =: c_a$ for $t \geq T_\varepsilon$. From Equations (B.86) to (B.88), with $\mu := 4\sigma^2 c_a^2$, we obtain $\tau\frac{d\mathcal{L}}{dt} \leq -\mu\mathcal{L}(t)$ and hence

$$\mathcal{L}(t) \leq \mathcal{L}(T_\varepsilon)e^{-\frac{\mu}{\tau}(t - T_\varepsilon)}. \tag{B.92}$$

Since $\mathcal{L}(t) \geq \sigma^2\|\boldsymbol{\theta} - \boldsymbol{\beta}\|^2$, we obtain

$$\|\boldsymbol{\theta}(t) - \boldsymbol{\beta}\| \leq \sqrt{\frac{\mathcal{L}(T_\varepsilon)}{\sigma^2}} e^{-\frac{\mu}{2\tau}(t - T_\varepsilon)}. \tag{B.93}$$

Since $|r_i(t)| = |\boldsymbol{v}_i^\top \boldsymbol{\Sigma}(\boldsymbol{\theta}(t) - \boldsymbol{\beta})| \leq \sigma^2(1 + \rho)\|\boldsymbol{\theta}(t) - \boldsymbol{\beta}\|$, there exists $C_{R2} > 0$ such that

$$\|\boldsymbol{R}(t)\| \leq C_{R2}\|\boldsymbol{\theta}(t) - \boldsymbol{\beta}\|. \tag{B.94}$$

Combining this with Inequality (B.93), we obtain

$$\|\boldsymbol{R}(t)\| \leq C_{R2}\sqrt{\frac{\mathcal{L}(T_\varepsilon)}{\sigma^2}} e^{-\frac{\mu}{2\tau}(t - T_\varepsilon)} =: C_{R3}e^{-\frac{\mu}{2\tau}(t - T_\varepsilon)}. \tag{B.95}$$

Now, from Equation (B.73), the deviation vector satisfies

$$\boldsymbol{e}_\perp(t) = \boldsymbol{e}_\perp(T_\varepsilon) + \frac{1}{\tau}\int_{T_\varepsilon}^{t} \boldsymbol{R}(t')\boldsymbol{e}_\perp(t')\,dt', \tag{B.96}$$

and therefore

$$\|\boldsymbol{e}_\perp(t)\| \le \|\boldsymbol{e}_\perp(T_\varepsilon)\| + \frac{1}{\tau}\int_{T_\varepsilon}^{t} \|\boldsymbol{R}(t')\|\|\boldsymbol{e}_\perp(t')\|\,dt'. \tag{B.97}$$

Applying Gronwall's inequality yields

$$\|\boldsymbol{e}_\perp(t)\| \le \|\boldsymbol{e}_\perp(T_\varepsilon)\| \exp\left(\frac{1}{\tau}\int_{T_\varepsilon}^{t} \|\boldsymbol{R}(t')\|\,dt'\right). \tag{B.98}$$

Thus, using Inequality (B.95), we have

$$\frac{1}{\tau}\int_{T_\varepsilon}^{t} \|\boldsymbol{R}(t')\|\,dt' \le \frac{C_{R3}}{\tau}\int_{T_\varepsilon}^{t} e^{-\frac{\mu}{2\tau}(t'-T_\varepsilon)}\,dt' = \frac{2C_{R3}}{\mu}\left(1 - e^{-\frac{\mu}{2\tau}(t-T_\varepsilon)}\right) \le \frac{2C_{R3}}{\mu}. \tag{B.99}$$

Also, since Step 1 gives $\|\boldsymbol{e}_\perp(T_\varepsilon)\| \le 2C_{e1}s$, the preceding two bounds imply

$$\sup_{t\in[T_\varepsilon,\infty)} \|\boldsymbol{e}_\perp(t)\| \le 2C_{e1}e^{2C_{R3}/\mu}s =: C_{e2}s. \tag{B.100}$$

Step 3: Combining the bounds. Combining Steps 1 and 2, and writing $C_{\boldsymbol{e}} := \max\{2C_{e1}, C_{e2}\}$, we obtain

$$\|\boldsymbol{e}_\perp(t)\| \le C_{\boldsymbol{e}}s. \tag{B.101}$$

Since $\boldsymbol{a} = \boldsymbol{u} + \boldsymbol{v}$ and $\boldsymbol{w}_1 = \boldsymbol{u} - \boldsymbol{v}$, it follows that

$$\|\boldsymbol{P}_\perp\boldsymbol{a}(t)\| + \|\boldsymbol{P}_\perp\boldsymbol{w}_1(t)\| + \|\boldsymbol{P}_\perp\boldsymbol{w}_2(t)\| \le 2\|\boldsymbol{P}_\perp\boldsymbol{u}(t)\| + 2\|\boldsymbol{P}_\perp\boldsymbol{v}(t)\| + \|\boldsymbol{P}_\perp\boldsymbol{w}_2(t)\| \le 3\|\boldsymbol{e}_\perp(t)\|. \tag{B.102}$$

Therefore, with $C_\perp := 3C_{\boldsymbol{e}}$, we obtain

$$\|\boldsymbol{P}_\perp\boldsymbol{a}(t)\| + \|\boldsymbol{P}_\perp\boldsymbol{w}_1(t)\| + \|\boldsymbol{P}_\perp\boldsymbol{w}_2(t)\| \le C_\perp s \tag{B.103}$$

for all $t \ge 0$. □

B.4 Derivation of the Two-Variable System (Proof of Theorem 3.3)

Building upon the global boundedness of the orthogonal components established in the previous subsection, we now provide the complete proof of Theorem 3.3. We demonstrate that the projected trajectory of the full system can be tightly approximated by the reduced two-variable dynamics, explicitly bounding the tracking error across all learning phases.

Proof of Theorem 3.3. Define

$$\tilde{a}(t) := \hat{\boldsymbol{r}}_1^\top\boldsymbol{a}(t), \quad \tilde{w}_1(t) := \hat{\boldsymbol{r}}_1^\top\boldsymbol{w}_1(t), \quad \tilde{w}_2(t) := \hat{\boldsymbol{r}}_1^\top\boldsymbol{w}_2(t). \tag{B.104}$$

By Lemma 3.2, the components orthogonal to $\hat{\boldsymbol{r}}_1$, as well as the modes $\boldsymbol{w}_i$ with $i \ge 3$, remain uniformly $O(s)$ for all $t \ge 0$. Thus, up to an $O(s)$ error, the full trajectory is captured by its projection onto $(\tilde{a}, \tilde{w}_1, \tilde{w}_2)$.

Effective Two-Variable Description of the Projected Exact Trajectory. By leveraging the bound $\left\|\boldsymbol{a}\boldsymbol{a}^\top - \sum_{i=1}^d \boldsymbol{w}_i\boldsymbol{w}_i^\top\right\| = O(s^2)$ together with $|\tilde{w}_i(t)| \leq \|\boldsymbol{w}_i(t)\| \leq \bar{c}s$ for all $i \geq 3$ and projecting the conservation law onto $\hat{\boldsymbol{r}}_1$, we obtain

$$\left|\tilde{a}(t)^2 - (\tilde{w}_1(t)^2 + \tilde{w}_2(t)^2)\right| \leq \sum_{i=3}^d |\tilde{w}_i(t)|^2 + \left\|\boldsymbol{a}\boldsymbol{a}^\top - \sum_{i=1}^d \boldsymbol{w}_i\boldsymbol{w}_i^\top\right\| \leq C_{\mathrm{tr}}^2 s^2. \tag{B.105}$$

Hence

$$\left|\tilde{a}(t) - \sqrt{\tilde{w}_1(t)^2 + \tilde{w}_2(t)^2}\right| \leq C_{\mathrm{tr}} s. \tag{B.106}$$

Thus, up to an $O(s)$ error, the projected exact state is effectively described by the two variables

$$\tilde{\boldsymbol{w}}(t) := (\tilde{w}_1(t), \tilde{w}_2(t))^\top. \tag{B.107}$$

Therefore, in the remainder of the proof we take $\tilde{\boldsymbol{w}}$ as the exact trajectory to be compared with the ideal reduced system, while $\tilde{a}$ is treated as the dependent quantity recovered from $\tilde{\boldsymbol{w}}$ through Inequality (B.106).

Ideal Reduced Trajectory. We define the subspace parametrized by three scalar functions $(a^\star(t), w_1^\star(t), w_2^\star(t))$ as follows:

$$\mathcal{M} = \{(\boldsymbol{a}, \boldsymbol{w}_1, \ldots, \boldsymbol{w}_d) : \boldsymbol{a} = a^\star\hat{\boldsymbol{r}}_1, \boldsymbol{w}_1 = w_1^\star\hat{\boldsymbol{r}}_1, \boldsymbol{w}_2 = w_2^\star\hat{\boldsymbol{r}}_1, \boldsymbol{w}_i = 0 \quad (i \geq 3)\}. \tag{B.108}$$

From Equations (9) to (12), if $(\boldsymbol{a}(0), \boldsymbol{w}_1(0), \ldots, \boldsymbol{w}_d(0)) \in \mathcal{M}$, then $(\boldsymbol{a}(t), \boldsymbol{w}_1(t), \ldots, \boldsymbol{w}_d(t)) \in \mathcal{M}$ for all $t \geq 0$. In addition, the conservation law implies $\frac{d}{dt}((a^\star)^2 - (w_1^\star)^2 - (w_2^\star)^2) = 0$.

Within this invariant set $\mathcal{M}$, we construct the ideal trajectory by defining the specific scalar components $(a(t), w_1(t), w_2(t))$. We set their initial conditions to precisely match the growing mode of the projected exact initialization:

$$a(0) = u_0 + \frac{q_0^2}{4u_0}, \quad w_1(0) = u_0 - \frac{q_0^2}{4u_0}, \quad w_2(0) = q_0 \tag{B.109}$$

where

$$u_0 := \hat{\boldsymbol{r}}_1^\top \frac{\boldsymbol{a}(0) + \boldsymbol{w}_1(0)}{2}, \quad q_0 := \hat{\boldsymbol{r}}_1^\top \boldsymbol{w}_2(0). \tag{B.110}$$

This initialization ensures that $a(0)^2 - w_1(0)^2 - w_2(0)^2 = 0$, which implies that $a(t)^2 = w_1(t)^2 + w_2(t)^2$ holds for all $t \geq 0$.

Since $a(0) > 0$, the sign of $a(t)$ could change only if $a(t_0) = 0$ for some t_0. In that case, necessarily $w_1(t_0) = w_2(t_0) = 0$, so the trajectory reaches the origin, which is an equilibrium of the system. Uniqueness of solutions for this rank-one system implies that the trajectory would have to remain at the origin for all later times, contradicting the nontrivial initialization. Hence $a(t) = \sqrt{w_1(t)^2 + w_2(t)^2}$ for all $t \geq 0$.

Consequently, the dynamics on $\mathcal{M}$ with the initial conditions given by Equation (B.109) are fully described by the two-dimensional vector

$$\boldsymbol{w}(t) := (w_1(t), w_2(t))^\top. \tag{B.111}$$

This exactly follows the dynamics of the reduced system (Equations (16) and (17)) with the initial condition in Equation (18).

Time Intervals and Proof Strategy. We compare the projected exact trajectory $\tilde{\boldsymbol{w}}$ and the ideal reduced trajectory $\boldsymbol{w}$ over three time intervals. Fix the small threshold ε from Equation (B.38) and set $\varepsilon_0 := \varepsilon/3$. Define

$$T_{\varepsilon_0} := \inf\left\{t \geq 0 : \max\{\|\tilde{\boldsymbol{w}}(t)\|, \|\boldsymbol{w}(t)\|\} \geq \varepsilon_0\right\}. \tag{B.112}$$

By construction, both trajectories remain within a small neighborhood of the origin on the interval $[0, T_{\varepsilon_0}]$.

Let $\boldsymbol{w}_\infty$ be the asymptotically stable equilibrium of the reduced two-variable system (Equations (16) and (17)). For any fixed $\varepsilon_\infty > 0$, we define the time at which the ideal trajectory enters an ε_∞-neighborhood of this equilibrium as:

$$T_{\varepsilon_\infty} := \inf\{t \geq 0 : \|\boldsymbol{w}(t) - \boldsymbol{w}_\infty\| \leq \varepsilon_\infty\}. \tag{B.113}$$

The proof is then divided into three steps. In Step 1, we analyze the near-origin dynamics on $[0, T_{\varepsilon_0}]$ by transforming the trajectories into lifted coordinates to decouple the growing and decaying modes. In Step 2 , we return to the two-variable coordinates to characterize the tracking error over the intermediate interval $[T_{\varepsilon_0}, T_{\varepsilon_\infty}]$. In Step 3, we use the asymptotic stability of $\boldsymbol{w}_\infty$ to control the error on the final interval $[T_{\varepsilon_\infty}, \infty)$.

Step 1: Bounding the dynamics on the interval $[0, T_{\varepsilon_0}]$. On the near-origin interval $[0, T_{\varepsilon_0}]$, we compare the two trajectories $\tilde{\boldsymbol{w}}$ and $\boldsymbol{w}$ after rewriting them in lifted coordinates that separate the growing and decaying modes.

For the projected exact trajectory $\tilde{\boldsymbol{w}}$, we define

$$\tilde{u}(t) := \frac{\tilde{a}(t) + \tilde{w}_1(t)}{2}, \quad \tilde{v}(t) := \frac{\tilde{a}(t) - \tilde{w}_1(t)}{2}, \quad \tilde{\boldsymbol{z}}(t) := (\tilde{u}(t), \tilde{v}(t), \tilde{w}_2(t))^\top. \tag{B.114}$$

Accordingly, projecting Equations (9), (10) and (12) onto $\hat{\boldsymbol{r}}_1$ and rewriting the result in the variables $\tilde{\boldsymbol{z}}$ yields

$$\tau \frac{d}{dt} \tilde{\boldsymbol{z}} = \boldsymbol{\Lambda} \tilde{\boldsymbol{z}} + \boldsymbol{h}(\tilde{\boldsymbol{z}}) + \boldsymbol{\xi}, \tag{B.115}$$

where $\boldsymbol{\Lambda} = \mathrm{diag}(\|\boldsymbol{\Sigma}_{xy}\|, -\|\boldsymbol{\Sigma}_{xy}\|, 0)$, and $\boldsymbol{h} : \mathbb{R}^3 \to \mathbb{R}^3$ denotes the explicit cubic polynomial vector field appearing in the lifted dynamics of the variables $(\tilde{u}, \tilde{v}, \tilde{w}_2)$. The vector $\boldsymbol{\xi} = (\xi_u, \xi_v, \xi_2)^\top$ collects all terms involving the orthogonal components and the remaining projected weights $\tilde{w}_i$ for $i \geq 3$. Since the original dynamics are cubic and the linear cross-terms between the parallel and orthogonal components vanish after projection onto $\hat{\boldsymbol{r}}_1$, each term in $\boldsymbol{\xi}$ contains at least two orthogonal or remaining factors, for instance $(\boldsymbol{P}_\perp \boldsymbol{w}_i)^\top (\boldsymbol{P}_\perp \boldsymbol{a})$ or $\tilde{w}_i^2$ with $i \geq 3$. Such terms are multiplied either by a parallel component $(\tilde{u}, \tilde{v}, \tilde{w}_2)$ or by another orthogonal or remaining component. Using Lemma 3.2 together with $\|\boldsymbol{w}_i(t)\| \leq \bar{c}s$ for $i \geq 3$, these components are uniformly $O(s)$, and hence the residual terms are bounded by $O(s^2|\tilde{u}|)$, $O(s^2|\tilde{v}|)$, $O(s^2|\tilde{w}_2|)$, and $O(s^3)$. Therefore, for all $t \geq 0$,

$$\|\boldsymbol{\xi}(t)\| \leq C_\xi s^2 (|\tilde{u}| + |\tilde{v}| + |\tilde{w}_2| + s). \tag{B.116}$$

For $t \in [0, T_{\varepsilon_0}]$, by definition we have $\|\tilde{\boldsymbol{w}}(t)\| \leq \varepsilon_0$, hence $|\tilde{w}_1(t)|, |\tilde{w}_2(t)| \leq \varepsilon_0$. In addition, Inequality (B.106) gives $|\tilde{a}(t)| \leq \sqrt{\tilde{w}_1(t)^2 + \tilde{w}_2(t)^2} + C_{\mathrm{tr}} s \leq 2\varepsilon_0$ for all sufficiently small s. Using Lemma 3.2 , we obtain

$$\|\boldsymbol{a}(t)\|, \|\boldsymbol{w}_1(t)\|, \|\boldsymbol{w}_2(t)\| \leq 2\varepsilon_0 + C_\perp s \leq \varepsilon \tag{B.117}$$

for all sufficiently small s, because $\varepsilon_0 = \varepsilon/3$. Therefore $[0, T_{\varepsilon_0}] \subset [0, T_\varepsilon]$, so Corollary B.6 applies throughout $[0, T_{\varepsilon_0}]$. Therefore,

$$|\tilde{u}(t)| \leq \|\boldsymbol{u}(t)\|, \quad |\tilde{v}(t)| \leq \|\boldsymbol{v}(t)\| \leq C_u \|\boldsymbol{u}(t)\|, \quad |\tilde{w}_2(t)| \leq \|\boldsymbol{w}_2(t)\| \leq C_u \|\boldsymbol{u}(t)\|. \tag{B.118}$$

Thus, using Inequality (B.118), we have

$$\|\tilde{\boldsymbol{z}}(t)\| \leq C_{\tilde{z}} \|\boldsymbol{u}(t)\|. \tag{B.119}$$

Also, substituting these bounds into Inequality (B.116), for $t \in [0, T_{\varepsilon_0}]$, we obtain

$$\|\boldsymbol{\xi}(t)\| \leq C_{\xi 1} s^2 \|\boldsymbol{u}(t)\|. \tag{B.120}$$

In addition, $\|\boldsymbol{u}(t)\| \leq (\|\boldsymbol{a}(t)\| + \|\boldsymbol{w}_1(t)\|)/2 \leq \varepsilon = 3\varepsilon_0$.

For the ideal reduced trajectory $\boldsymbol{w}$, we set

$$u(t) := \frac{\sqrt{w_1(t)^2 + w_2(t)^2} + w_1(t)}{2}, \quad v(t) := \frac{\sqrt{w_1(t)^2 + w_2(t)^2} - w_1(t)}{2}, \tag{B.121}$$

$$\boldsymbol{z}(t) := (u(t), v(t), w_2(t))^\top. \tag{B.122}$$

Since the ideal reduced trajectory $\boldsymbol{z}$ is a special case of the general dynamics where all orthogonal components and the remaining weights $\boldsymbol{w}_i$ for $i \geq 3$ are identically zero, its lifted dynamics are governed by the exact same differential equations as Equation (B.115) but without the residual error term $\boldsymbol{\xi}$. Therefore,

$$\tau \frac{d}{dt}\boldsymbol{z} = \boldsymbol{\Lambda}\boldsymbol{z} + \boldsymbol{h}(\boldsymbol{z}). \tag{B.123}$$

The arguments of Lemmas B.4 and B.5 and the proof of Corollary B.6 also apply directly to (u, v, w_2) on $[0, T_{\varepsilon_0}]$, with the same constant $c_1 = \|\boldsymbol{\Sigma}_{xy}\| - C_0\varepsilon^2$. In particular, the following inequalities hold:

$$0 \leq v(t) \leq u(t), \quad \tau\frac{d}{dt}u(t) \geq c_1 u(t), \tag{B.124}$$

$$\|\boldsymbol{z}(t)\| \leq C_z u(t), \tag{B.125}$$

and $u(t) \leq \varepsilon_0$.

Let $\boldsymbol{e}_z := \tilde{\boldsymbol{z}} - \boldsymbol{z}$ and $\bar{e}_z(t) := \sup_{t' \in [0,t]} \|\boldsymbol{e}_z(t')\|$. Subtracting Equation (B.123) from Equation (B.115), we obtain

$$\tau\frac{d}{dt}\boldsymbol{e}_z = \boldsymbol{\Lambda}\boldsymbol{e}_z + (\boldsymbol{h}(\tilde{\boldsymbol{z}}) - \boldsymbol{h}(\boldsymbol{z})) + \boldsymbol{\xi}. \tag{B.126}$$

The variation of constants formula gives

$$\boldsymbol{e}_z(t) = e^{\boldsymbol{\Lambda}t/\tau}\boldsymbol{e}_z(0) + \frac{1}{\tau}\int_0^t e^{\boldsymbol{\Lambda}(t-t')/\tau}(\boldsymbol{h}(\tilde{\boldsymbol{z}}(t')) - \boldsymbol{h}(\boldsymbol{z}(t')) + \boldsymbol{\xi}(t'))\, dt'. \tag{B.127}$$

For the first term, we have

$$e^{\boldsymbol{\Lambda}t/\tau}\boldsymbol{e}_z(0) = (0, (\tilde{v}(0) - v(0))e^{-\|\boldsymbol{\Sigma}_{xy}\|t/\tau}, 0)^\top, \tag{B.128}$$

and hence

$$\|e^{\boldsymbol{\Lambda}t/\tau}\boldsymbol{e}_z(0)\| \leq C_{z1}s. \tag{B.129}$$

Since $\boldsymbol{h}$ is cubic, the integral form of the mean-value theorem together with Inequalities (B.119) and (B.125) yields

$$\|\boldsymbol{h}(\tilde{\boldsymbol{z}}) - \boldsymbol{h}(\boldsymbol{z})\| \leq C_h(\|\boldsymbol{u}\|^2 + u^2)\|\boldsymbol{e}_z\|. \tag{B.130}$$

Taking norms the second term in Equation (B.127) and using Inequalities (B.120) and (B.130), we obtain

$$\begin{aligned}&\left\|\frac{1}{\tau}\int_0^t e^{\boldsymbol{\Lambda}(t-t')/\tau}(\boldsymbol{h}(\tilde{\boldsymbol{z}}(t')) - \boldsymbol{h}(\boldsymbol{z}(t')) + \boldsymbol{\xi}(t'))\, dt'\right\| \\ &\qquad \leq C_h\bar{e}_z(t)\frac{1}{\tau}\int_0^t e^{\|\boldsymbol{\Sigma}_{xy}\|(t-t')/\tau}(\|\boldsymbol{u}(t')\|^2 + (u(t'))^2)\, dt' + C_{\xi 1}s^2\frac{1}{\tau}\int_0^t e^{\|\boldsymbol{\Sigma}_{xy}\|(t-t')/\tau}\|\boldsymbol{u}(t')\|\, dt'.\end{aligned} \tag{B.131}$$

Let $\alpha := \|\boldsymbol{\Sigma}_{xy}\|/c_1 = \|\boldsymbol{\Sigma}_{xy}\|/(\|\boldsymbol{\Sigma}_{xy}\| - C_0\varepsilon^2) \in (1, 2)$, where the inclusion follows by choosing ε sufficiently small. Since $T_{\varepsilon_0} \leq T_\varepsilon$, Inequality (B.40) gives $\tau\frac{d}{dt}\|\boldsymbol{u}\| \geq c_1\|\boldsymbol{u}\|$, and Inequality (B.124) gives the same inequality for u. Applying Lemma B.2 with $(x, \gamma, \beta, p) = (\|\boldsymbol{u}\|, c_1, \|\boldsymbol{\Sigma}_{xy}\|, 2)$, $(u, c_1, \|\boldsymbol{\Sigma}_{xy}\|, 2)$, and $(\|\boldsymbol{u}\|, c_1, \|\boldsymbol{\Sigma}_{xy}\|, 1)$, respectively, we obtain

$$\frac{1}{\tau}\int_0^t e^{\|\boldsymbol{\Sigma}_{xy}\|(t-t')/\tau}\|\boldsymbol{u}(t')\|^2\, dt' \leq \frac{\|\boldsymbol{u}(t)\|^2}{2c_1 - \|\boldsymbol{\Sigma}_{xy}\|} \leq C_{u2}\varepsilon_0^2, \tag{B.132}$$

$$\frac{1}{\tau}\int_0^t e^{\|\boldsymbol{\Sigma}_{xy}\|(t-t')/\tau}u(t')^2\, dt' \leq \frac{u(t)^2}{2c_1 - \|\boldsymbol{\Sigma}_{xy}\|} \leq C_{u3}\varepsilon_0^2, \tag{B.133}$$

$$s^2\frac{1}{\tau}\int_0^t e^{\|\boldsymbol{\Sigma}_{xy}\|(t-t')/\tau}\|\boldsymbol{u}(t')\|\, dt' \leq C_{\xi 1}\varepsilon_0^\alpha s^{3-\alpha}. \tag{B.134}$$

Here the first two lines use the second case of Lemma B.2, together with $\|\boldsymbol{u}(t)\|^2 \le 9\varepsilon_0^2$, while the third line uses the first case with $\|\boldsymbol{u}(t)\| \le 3\varepsilon_0$ and $\|\boldsymbol{u}(0)\| = c_{u0}s$.

Using Equation (B.127), Inequality (B.129), and Inequalities (B.132) to (B.134) in Inequality (B.131), we obtain

$$\overline{e}_z(t) \le C_{z1}s + C_{h1}\varepsilon_0^2\overline{e}_z(t) + C_{\xi 1}\varepsilon_0^{\alpha}s^{3-\alpha}. \tag{B.135}$$

Choosing ε_0 sufficiently small so that $C_{h1}\varepsilon_0^2 \le 1/2$, and recalling that $\alpha \in (1,2)$, we obtain, for all $t \in [0, T_{\varepsilon_0}]$,

$$\overline{e}_z(t) \le C_z s. \tag{B.136}$$

Since $\tilde{w}_1 - w_1 = (\tilde{u} - u) - (\tilde{v} - v)$ and $\tilde{w}_2 - w_2 = \tilde{w}_2 - w_2$, Inequality (B.136) immediately implies, for all $t \in [0, T_{\varepsilon_0}]$,

$$\|\tilde{\boldsymbol{w}}(t) - \boldsymbol{w}(t)\| \le C_{w1}s. \tag{B.137}$$

Step 2: Bounding the dynamics over the intermediate interval $[T_{\varepsilon_0}, T_{\varepsilon_\infty}]$. We now return to the two-variable coordinates. Define $\boldsymbol{F} : \mathbb{R}^2 \to \mathbb{R}^2$ by

$$\boldsymbol{F}(x_1, x_2) := \begin{pmatrix} \|\boldsymbol{\Sigma}_{xy}\|\sqrt{x_1^2 + x_2^2} - \lambda_1 x_1(x_1^2 + x_2^2) + \nu x_2(x_1^2 + x_2^2) \\ \nu x_1(x_1^2 + x_2^2) - \lambda_2 x_2(x_1^2 + x_2^2) \end{pmatrix}. \tag{B.138}$$

Then the reduced two-variable dynamics and the projected full-system dynamics take the form

$$\tau\frac{d}{dt}\boldsymbol{w} = \boldsymbol{F}(\boldsymbol{w}), \tag{B.139}$$

$$\tau\frac{d}{dt}\tilde{\boldsymbol{w}} = \boldsymbol{F}(\tilde{\boldsymbol{w}}) + \boldsymbol{\zeta}(t), \tag{B.140}$$

where the total error term is $\boldsymbol{\zeta}(t) := \boldsymbol{E}_a(t) + \hat{\boldsymbol{\xi}}(t)$ with

$$\boldsymbol{E}_a(t) := \begin{pmatrix} \|\boldsymbol{\Sigma}_{xy}\|(\tilde{a} - \sqrt{\tilde{w}_1^2 + \tilde{w}_2^2}) - \lambda_1\tilde{w}_1(\tilde{a}^2 - (\tilde{w}_1^2 + \tilde{w}_2^2)) + \nu\tilde{w}_2(\tilde{a}^2 - (\tilde{w}_1^2 + \tilde{w}_2^2)) \\ \nu\tilde{w}_1(\tilde{a}^2 - (\tilde{w}_1^2 + \tilde{w}_2^2)) - \lambda_2\tilde{w}_2(\tilde{a}^2 - (\tilde{w}_1^2 + \tilde{w}_2^2)) \end{pmatrix} \tag{B.141}$$

and $\hat{\boldsymbol{\xi}}(t) := (\xi_u(t) - \xi_v(t), \xi_2(t))^\top$.

Let $\boldsymbol{e}(t) := \tilde{\boldsymbol{w}}(t) - \boldsymbol{w}(t)$. Subtracting Equation (B.139) from Equation (B.140), we obtain

$$\tau\frac{d}{dt}\boldsymbol{e} = \boldsymbol{F}(\tilde{\boldsymbol{w}}) - \boldsymbol{F}(\boldsymbol{w}) + \boldsymbol{\zeta}(t). \tag{B.142}$$

Because $\boldsymbol{w}(t)$ reaches the ε_∞-neighborhood of $\boldsymbol{w}_\infty$ in $O(1)$ time and $\boldsymbol{F}$ has no critical points outside that neighborhood, the interval length $T_{\varepsilon_\infty} - T_{\varepsilon_0}$ is bounded independently of s. Since both trajectories remain in a compact set away from the origin on $[T_{\varepsilon_0}, T_{\varepsilon_\infty}]$, $\boldsymbol{F}$ is Lipschitz along this interval. Hence there exists $L_{\varepsilon_0,\varepsilon_\infty} > 0$ such that $\|\boldsymbol{F}(\tilde{\boldsymbol{w}}) - \boldsymbol{F}(\boldsymbol{w})\| \le L_{\varepsilon_0,\varepsilon_\infty}\|\tilde{\boldsymbol{w}} - \boldsymbol{w}\|$ on $[T_{\varepsilon_0}, T_{\varepsilon_\infty}]$. Also, there exists $\delta_{\varepsilon_0,\varepsilon_\infty} > 0$ such that $\|\tilde{\boldsymbol{w}}(t)\|, \|\boldsymbol{w}(t)\| \ge \delta_{\varepsilon_0,\varepsilon_\infty}$ throughout this interval. For sufficiently small s, Inequality (B.106) then forces $\tilde{a}(t) > 0$, so $|\tilde{a}(t) - \sqrt{\tilde{w}_1(t)^2 + \tilde{w}_2(t)^2}| \le C_{\mathrm{tr}}s$. Since $\tilde{\boldsymbol{w}}$ remains bounded, Inequality (B.105) gives $\|\boldsymbol{E}_a(t)\| \le C'_{E_a}(|\tilde{a}(t) - \sqrt{\tilde{w}_1(t)^2 + \tilde{w}_2(t)^2}| + |\tilde{a}(t)^2 - (\tilde{w}_1(t)^2 + \tilde{w}_2(t)^2)|) \le C_{E_a}s$, while Inequality (B.116) and the fact that the lifted variables $(\tilde{u}(t), \tilde{v}(t), \tilde{w}_2(t))$ remain uniformly bounded on $[T_{\varepsilon_0}, T_{\varepsilon_\infty}]$ imply $\|\hat{\boldsymbol{\xi}}(t)\| \le C_{\xi 2}s^2$. Hence

$$\|\boldsymbol{\zeta}(t)\| \le \|\boldsymbol{E}_a(t)\| + \|\hat{\boldsymbol{\xi}}(t)\| \le C_{\zeta 2}s \tag{B.143}$$

for some constant $C_{\zeta 2} > 0$.

Applying Gronwall's inequality on $[T_{\varepsilon_0}, t]$ yields

$$\|\boldsymbol{e}(t)\| \le \|\boldsymbol{e}(T_{\varepsilon_0})\|e^{L_{\varepsilon_0,\varepsilon_\infty}(t - T_{\varepsilon_0})/\tau} + \frac{C_{\zeta 2}s}{L_{\varepsilon_0,\varepsilon_\infty}}\left(e^{L_{\varepsilon_0,\varepsilon_\infty}(t - T_{\varepsilon_0})/\tau} - 1\right). \tag{B.144}$$

From the conclusion of Step 1, we have the initial error bound $\|\boldsymbol{e}(T_{\varepsilon_0})\| \leq C_{\varepsilon_0} s$ for some $C_{\varepsilon_0} > 0$. Since the transit time is bounded, the exponential factor is uniformly $O(1)$ on $[T_{\varepsilon_0}, T_{\varepsilon_\infty}]$. Therefore, the error remains bounded by a constant multiple of s throughout the entire intermediate interval:

$$\|\boldsymbol{e}(t)\| \leq C_{w2} s \tag{B.145}$$

for some constant $C_{w2} > 0$.

Step 3: Bounding the dynamics over the infinite horizon $[T_{\varepsilon_\infty}, \infty)$**.** By step 2, Equation (B.140) may be viewed as a perturbation of Equation (B.139), with forcing term satisfying $\|\boldsymbol{\zeta}(t)\| \leq C_{\zeta 3} s$ uniformly for all $t \geq T_{\varepsilon_\infty}$.

Since $\boldsymbol{w}_\infty$ is an exponentially stable equilibrium of the reduced two-variable system, standard perturbation results for exponentially stable systems (Khalil (2002), Theorem 4.14 and Lemma 9.2) imply that, for all $t \geq T_{\varepsilon_\infty}$, the tracking error satisfies

$$\|\tilde{\boldsymbol{w}}(t) - \boldsymbol{w}(t)\| \leq C_{w3} s. \tag{B.146}$$

Step 4: Combining the bounds. Combining the bounds over the three intervals from Steps 1 to 3, there exists a constant $C_\parallel > 0$ such that, for all $t \geq 0$,

$$\|\tilde{\boldsymbol{w}}(t) - \boldsymbol{w}(t)\| \leq C_\parallel s. \tag{B.147}$$

The global relation Inequality (B.106) then gives

$$\left|\tilde{a}(t) - \sqrt{w_1(t)^2 + w_2(t)^2}\right| \leq \left|\tilde{a}(t) - \sqrt{\tilde{w}_1(t)^2 + \tilde{w}_2(t)^2}\right| + \|\tilde{\boldsymbol{w}}(t) - \boldsymbol{w}(t)\| \leq (C_{\mathrm{tr}} + C_\parallel) s \tag{B.148}$$

for all $t \geq 0$. Recall that the actual trajectories in the full network can be decomposed into the projected components and the orthogonal components, i.e., $\boldsymbol{w}_i(t) = \tilde{w}_i(t)\hat{\boldsymbol{r}}_1 + \boldsymbol{P}_\perp \boldsymbol{w}_i(t)$ and $\boldsymbol{a}(t) = \tilde{a}(t)\hat{\boldsymbol{r}}_1 + \boldsymbol{P}_\perp \boldsymbol{a}(t)$. The orthogonal components are globally bounded by $\|\boldsymbol{P}_\perp \boldsymbol{a}(t)\|, \|\boldsymbol{P}_\perp \boldsymbol{w}_i(t)\| \leq C_\perp s$ from Lemma 3.2. Applying the triangle inequality to these parallel and orthogonal bounds directly yields the final statement of the theorem:

$$\|\boldsymbol{w}_1(t) - \hat{\boldsymbol{r}}_1 w_1(t)\| \leq Cs, \quad \|\boldsymbol{w}_2(t) - \hat{\boldsymbol{r}}_1 w_2(t)\| \leq Cs, \quad \left\|\boldsymbol{a}(t) - \hat{\boldsymbol{r}}_1 \sqrt{w_1(t)^2 + w_2(t)^2}\right\| \leq Cs. \tag{B.149}$$

□

C Analysis of the Reduced Dynamics

In this section, we provide a detailed analysis of the reduced dynamics.

C.1 Early Phase

In this subsection, to rigorously bound the trajectories and ensure that the linear driving force strictly dominates the interaction terms, we introduce a constant R satisfying $\|\boldsymbol{\Sigma}_{xy}\| - \lambda_1 R^2 > 0$ and then define an exit time $T_R = \inf\{t \geq 0 : w_1(t)^2 + w_2(t)^2 \geq R^2\}$.

Furthermore, we define the region $\Omega_{B_1,B_2} = \{(w_1, w_2) : w_1 \geq -B_1 s, w_2 \geq -B_2 s\}$. Here, B_1 and B_2 are positive constants chosen so that $(w_1(0), w_2(0)) \in \Omega_{B_1,B_2}$ and satisfy $-\nu B_1 + \lambda_2 B_2 > 0$. This region is used only as an auxiliary device in the proof below.

The subsequent statements in this subsection restrict the analysis to the interval $t \in [0, T_R)$. We show that our analytical approximations for the early phase dynamics hold as long as the weights remain within this boundary.

C.1.1 Bounding the Component w_2 (Proof of Proposition 3.4)

Lemma C.1. *Let B_1 and B_2 be positive constants such that $(w_1(0), w_2(0)) \in \Omega_{B_1,B_2}$ and $-\nu B_1 + \lambda_2 B_2 > 0$. Then for all sufficiently small $s > 0$, and all $t \geq 0$, we have $(w_1(t), w_2(t)) \in \Omega_{B_1,B_2}$.*

Proof. Suppose there exists a first exit time $t^* = \inf\{t \geq 0 : (w_1(t), w_2(t)) \notin \Omega_{B_1,B_2}\}$. Then, by continuity of $(w_1(t), w_2(t))$, we have $(w_1(t^*), w_2(t^*)) \in \partial\Omega_{B_1,B_2}$. At this time, the trajectory must leave Ω_{B_1,B_2} through either the left boundary $w_1 = -B_1 s$ or the lower boundary $w_2 = -B_2 s$.

First, consider the case where $w_1(t^*) \geq -B_1 s$ and $w_2(t^*) = -B_2 s$. Evaluating Equation (17) at $t = t^*$ and using $-\nu B_1 + \lambda_2 B_2 > 0$, we obtain

$$\begin{aligned} \tau\frac{d}{dt}w_2(t^*) &= (w_1(t^*)^2 + w_2(t^*)^2)(\nu w_1(t^*) - \lambda_2 w_2(t^*)) \\ &\geq (w_1(t^*)^2 + w_2(t^*)^2)(-\nu B_1 + \lambda_2 B_2)s \\ &> 0. \end{aligned} \tag{C.1}$$

Hence the trajectory cannot cross the boundary $w_2 = -B_2 s$ from inside to outside at time t^*, which is a contradiction.

Next, consider the case where $w_1(t^*) = -B_1 s$ and $w_2(t^*) \geq -B_2 s$. If $w_2(t^*) \geq 0$, then

$$\tau\frac{d}{dt}w_1(t^*) \geq \|\mathbf{\Sigma}_{xy}\|\sqrt{w_1(t^*)^2 + w_2(t^*)^2} \geq \|\mathbf{\Sigma}_{xy}\|B_1 s > 0. \tag{C.2}$$

If $-B_2 s \leq w_2(t^*) < 0$, then $w_1(t^*)^2 + w_2(t^*)^2 \leq (B_1^2 + B_2^2)s^2$, and hence

$$\begin{aligned} \tau\frac{d}{dt}w_1(t^*) &= \|\mathbf{\Sigma}_{xy}\|\sqrt{w_1(t^*)^2 + w_2(t^*)^2} + (\lambda_1 B_1 s + \nu w_2(t^*))(w_1(t^*)^2 + w_2(t^*)^2) \\ &\geq \|\mathbf{\Sigma}_{xy}\|B_1 s - \nu B_2(B_1^2 + B_2^2)s^3. \end{aligned} \tag{C.3}$$

Therefore, for all sufficiently small $s > 0$, we have $dw_1(t^*)/dt > 0$. Thus the trajectory cannot cross the boundary $w_1 = -B_1 s$ from inside to outside at time t^*, again a contradiction.

Since neither boundary can be crossed from inside to outside, the assumed exit time t^* cannot exist. Therefore,

$$(w_1(t), w_2(t)) \in \Omega_{B_1,B_2} \tag{C.4}$$

for all $t \geq 0$. □

Lemma C.2. *Let B_1 and B_2 be as in Lemma C.1. Then, for all sufficiently small $s > 0$, and all $t \in [0, T_R)$, we have*

$$\tau\frac{d}{dt}w_1 \geq \frac{1}{2}(\|\mathbf{\Sigma}_{xy}\| - \lambda_1 R^2)\sqrt{w_1^2 + w_2^2} > 0. \tag{C.5}$$

Proof. From Equation (16), using $(w_1, w_2) \in \Omega_{B_1,B_2}$ and $\sqrt{w_1^2 + w_2^2} \leq R$, for a sufficiently small $s > 0$, we have

$$\begin{aligned} \tau\frac{d}{dt}w_1 &= \left(\|\mathbf{\Sigma}_{xy}\| - \lambda_1 w_1\sqrt{w_1^2 + w_2^2} + \nu w_2\sqrt{w_1^2 + w_2^2}\right)\sqrt{w_1^2 + w_2^2} \\ &\geq (\|\mathbf{\Sigma}_{xy}\| - \lambda_1 R^2 - \nu B_2 R s)\sqrt{w_1^2 + w_2^2} \\ &\geq \frac{1}{2}(\|\mathbf{\Sigma}_{xy}\| - \lambda_1 R^2)\sqrt{w_1^2 + w_2^2} \\ &> 0. \end{aligned} \tag{C.6}$$

Note that the strict inequality holds because the origin $(w_1, w_2) = (0, 0)$ is a fixed point of the system. By the uniqueness of solutions to ODEs, a trajectory starting from a non-zero initialization cannot reach the origin in finite time, ensuring $\sqrt{w_1^2 + w_2^2} > 0$. □

Lemma C.3. *Let B_1 and B_2 be as in Lemma C.1. Then, there exists a constant $K > 0$ such that, for all sufficiently small $s > 0$ and all $t \in [0, T_R)$,*

$$w_2(t) \leq \frac{2\nu\sqrt{1 + (\nu/\lambda_2)^2}}{3(\|\mathbf{\Sigma}_{xy}\| - \lambda_1 R^2)} w_1(t)^3 + Ks. \tag{C.7}$$

Proof. First, observe that if $\nu w_1/\lambda_2 \leq w_2$, we trivially have $\tau dw_2 \leq 0$. Since $\tau dw_1/dt > 0$ from Lemma C.2, this implies $dw_2/dw_1 \leq 0$. Thus, for the purpose of upper-bounding dw_2/dw_1, we only need to consider the region where $\tau dw_2/dt > 0$, which strictly requires $w_2 < \nu w_1/\lambda_2$.

Assuming $w_2 < \nu w_1/\lambda_2$, since $(w_1, w_2) \in \Omega_{B_1,B_2}$, we also have $-w_2 \leq B_2 s$. Therefore,

$$\tau \frac{dw_2}{dt} = (w_1^2 + w_2^2)(\nu w_1 - \lambda_2 w_2) \leq (w_1^2 + w_2^2)(\nu w_1 + \lambda_2 B_2 s). \tag{C.8}$$

We now bound this expression by dividing into two cases based on the sign of w_1.

First, we consider the case where $-B_1 s \leq w_1 < 0$. Since $w_1 < 0$, we have $\nu w_1 + \lambda_2 B_2 s < \lambda_2 B_2 s$. Combining this with $\sqrt{w_1^2 + w_2^2} \leq R$, we obtain

$$\tau \frac{dw_2}{dt} \leq \lambda_2 B_2 s (w_1^2 + w_2^2) \leq \lambda_2 B_2 R s \sqrt{w_1^2 + w_2^2}. \tag{C.9}$$

Next, we consider the case where $0 \leq w_1$. In this region, w_2 is bounded by $-B_2 s \leq w_2 < \nu w_1/\lambda_2$. Therefore,

$$\sqrt{w_1^2 + w_2^2} \leq \sqrt{w_1^2 + \max\left(B_2 s, \frac{\nu}{\lambda_2} w_1\right)^2} \leq w_1 \sqrt{1 + \left(\frac{\nu}{\lambda_2}\right)^2} + B_2 s. \tag{C.10}$$

Substituting this into Equation (C.8), we have

$$\begin{aligned} \tau \frac{dw_2}{dt} &\leq \sqrt{w_1^2 + w_2^2} \left(w_1 \sqrt{1 + \left(\frac{\nu}{\lambda_2}\right)^2} + B_2 s \right) (\nu w_1 + \lambda_2 B_2 s) \\ &\leq \left(\nu \sqrt{1 + \left(\frac{\nu}{\lambda_2}\right)^2} w_1^2 + B_3 s \right) \sqrt{w_1^2 + w_2^2} \end{aligned} \tag{C.11}$$

where $B_3 \geq \lambda_2 B_2 R$ is a constant. Here, the cross terms $O(s w_1)$ are absorbed into the $O(s)$ term since $w_1 \leq R$. Note that this bound also encompasses the first case.

Therefore, dividing by Equation (C.5), we have

$$\frac{dw_2}{dw_1} \leq \frac{2\nu\sqrt{1 + (\nu/\lambda_2)^2}}{\|\mathbf{\Sigma}_{xy}\| - \lambda_1 R^2} w_1^2 + B_3 s. \tag{C.12}$$

for all $t \in [0, T_R)$. Integrating this differential inequality with respect to w_1 from $w_1(0)$ to $w_1(t)$, we obtain

$$w_2(t) - w_2(0) \leq \frac{2\nu\sqrt{1 + (\nu/\lambda_2)^2}}{3(\|\mathbf{\Sigma}_{xy}\| - \lambda_1 R^2)} (w_1(t)^3 - w_1(0)^3) + B_3 s (w_1(t) - w_1(0)) \tag{C.13}$$

Since $w_1(t) < R$ for all $t \in [0, T_R)$ and the initialization satisfies $w_1(0) = O(s)$ and $w_2(0) = O(s)$, the remaining terms on the right-hand side are all of order $O(s)$. Therefore, they can be absorbed into a single term Ks for some constant $K > 0$, yielding Equation (C.7). □

Proof of Proposition 3.4. From the definition of Ω_{B_1,B_2}, we have the lower bound $w_2(t) \geq -B_2 s$. Combining this with the upper bound provided by Lemma C.3 and defining $C = \max\{K, B_2\}$, we immediately obtain

$$|w_2(t)| \leq \frac{2\nu\sqrt{1 + (\nu/\lambda_2)^2}}{3(\|\mathbf{\Sigma}_{xy}\| - \lambda_1 R^2)} |w_1(t)|^3 + Cs. \tag{C.14}$$

for all $t \in [0, T_R)$. □

C.1.2 Decoupled Dynamics of the Component w_1 (Proof of Proposition 3.5)

Building on the suppression of w_2 established above, we demonstrate that the evolution of w_1 can be effectively decoupled and approximated by a one-dimensional differential equation.

Proof of Proposition 3.5. We rewrite Equation (16) as:

$$\tau \frac{d}{dt} w_1(t) = \|\mathbf{\Sigma}_{xy}\| w_1(t) - \lambda_1 w_1(t)^3 + \varepsilon_R(t) \tag{C.15}$$

where

$$\varepsilon_R(t) = \|\mathbf{\Sigma}_{xy}\| \left(\sqrt{w_1^2 + w_2^2} - w_1 \right) - \lambda_1 w_1 w_2^2 + \nu w_2 (w_1^2 + w_2^2). \tag{C.16}$$

Therefore,

$$|\varepsilon_R(t)| \leq \|\mathbf{\Sigma}_{xy}\| \left| \sqrt{w_1^2 + w_2^2} - w_1 \right| + \lambda_1 |w_1| |w_2|^2 + \nu |w_2| (|w_1|^2 + |w_2|^2). \tag{C.17}$$

By Proposition 3.4, there exist constants $K_1, K_2 > 0$ such that $|w_2| \leq K_1 |w_1|^3 + K_2 s$ for all $t \in [0, T_R)$. By the definition of Ω_{B_1,B_2}, we have $w_1 \geq -B_1 s$. If $|w_1| \leq B_1 s$, we have

$$\left| \sqrt{w_1^2 + w_2^2} - w_1 \right| \leq \sqrt{w_1^2 + w_2^2} + |w_1| \leq 2|w_1| + |w_2| \leq 2B_1 s + K_1 B_1^3 s^3 + K_2 s \leq M_1 s. \tag{C.18}$$

If $w_1 > B_1 s$, then $w_1 > 0$ and hence

$$\left| \sqrt{w_1^2 + w_2^2} - w_1 \right| = \sqrt{w_1^2 + w_2^2} - w_1 = \frac{w_2^2}{\sqrt{w_1^2 + w_2^2} + w_1} \leq \frac{w_2^2}{2w_1} \leq M_2 w_1^5 + M_3 s. \tag{C.19}$$

Moreover, the remaining two terms are bounded by $M_4 |w_1|^5 + M_5 s$, together with the early-phase bound $w_1^2 + w_2^2 < R^2$. Combining these bounds yields

$$|\varepsilon_R(t)| \leq C_1 |w_1|^5 + C_2 s \tag{C.20}$$

for some constants $C_1, C_2 > 0$. □

C.1.3 Derivation of the Early Phase Timescale

Using the decoupled dynamics, we derive an explicit analytical approximation for the growth of w_1 and quantify the characteristic timescale of its sigmoidal transition.

From Proposition 3.5, if we neglect the remainder term $\varepsilon_R(t)$, we can define an idealized approximation of the trajectory, denoted by $w_1^{(0)}(t)$, which strictly follows the truncated dynamics:

$$\tau \frac{d}{dt} w_1^{(0)}(t) = \|\mathbf{\Sigma}_{xy}\| w_1^{(0)}(t) - \lambda_1 w_1^{(0)}(t)^3. \tag{C.21}$$

Solving this Bernoulli differential equation with the initial condition $w_1^{(0)}(0) = w_1(0)$ gives the exact closed-form solution:

$$w_1^{(0)}(t) = \sqrt{\frac{\|\mathbf{\Sigma}_{xy}\|}{\lambda_1} \left(1 + \left(\frac{\|\mathbf{\Sigma}_{xy}\|/\lambda_1}{w_1(0)^2} - 1 \right) e^{-\frac{2\|\mathbf{\Sigma}_{xy}\|}{\tau} t} \right)^{-1}}. \tag{C.22}$$

As long as the residual $\varepsilon_R(t)$ remains small, this idealized solution closely tracks the true magnitude $w_1(t)$.

Let

$$w_{1\infty}^{(0)} := \sqrt{\frac{\|\mathbf{\Sigma}_{xy}\|}{\lambda_1}} \tag{C.23}$$

denote the asymptotic saturation value. To quantify the sigmoidal transition, fix any fraction $0 < p < 1$ and define t_p as the time at which the approximation reaches this fraction:

$$w_1^{(0)}(t_p) = p w_{1\infty}^{(0)}. \tag{C.24}$$

Substituting this into Equation (C.22) gives

$$p^2 = \left(1 + \left(\frac{(w_{1\infty}^{(0)})^2}{w_1(0)^2} - 1\right) e^{-\frac{2\|\mathbf{\Sigma}_{xy}\|}{\tau} t_p}\right)^{-1}, \tag{C.25}$$

hence

$$t_p = \frac{\tau}{2\|\mathbf{\Sigma}_{xy}\|} \log\left[\left(\frac{(w_{1\infty}^{(0)})^2}{w_1(0)^2} - 1\right) \frac{p^2}{1-p^2}\right]. \tag{C.26}$$

Using $(w_{1\infty}^{(0)})^2 = \|\mathbf{\Sigma}_{xy}\|/\lambda_1$, this can be rewritten as

$$t_p = \frac{\tau}{2\|\mathbf{\Sigma}_{xy}\|} \log\left[\left(\frac{\|\mathbf{\Sigma}_{xy}\|}{\lambda_1 w_1(0)^2} - 1\right) \frac{p^2}{1-p^2}\right]. \tag{C.27}$$

When the initialization is small, with $w_1(0) = \Theta(s)$ for $s \ll 1$, the argument of the logarithm is dominated by the term $\|\mathbf{\Sigma}_{xy}\|/(\lambda_1 w_1(0)^2) \gg 1$. Thus, for any fixed fraction $p \in (0,1)$, the time t_p can be asymptotically expanded as:

$$t_p = \frac{\tau}{2\|\mathbf{\Sigma}_{xy}\|} \log\left(\frac{\|\mathbf{\Sigma}_{xy}\|}{\lambda_1 w_1(0)^2}\right) + O(1). \tag{C.28}$$

Expressing this in terms of the initialization scale s, the leading term is:

$$\frac{\tau}{2\|\mathbf{\Sigma}_{xy}\|} \log\left(\frac{\|\mathbf{\Sigma}_{xy}\|}{\lambda_1 s^2}\right). \tag{C.29}$$

Crucially, the choice of the specific fraction p affects only the additive $O(1)$ constant, leaving the leading-order logarithmic scaling invariant. This justifies the characteristic timescale for the early phase presented in the main text.

C.2 Later Phase

In this subsection, we provide the derivation of the upper bound on the timescale for the later phase given in the main text.

C.2.1 Derivation of the Later Phase Timescale (Proof of Proposition 3.6)

Proof of Proposition 3.6. Under the assumptions, we have $w_1(t) \geq w_{1\infty}$ and $w_2(t) \leq w_{2\infty}$. Using these inequalities, we can establish a lower bound on the derivative of w_2:

$$\tau \frac{dw_2}{dt} = (w_1^2 + w_2^2)(\nu w_1 - \lambda_2 w_2) \geq (w_{1\infty}^2 + w_2^2)(\nu w_{1\infty} - \lambda_2 w_2). \tag{C.30}$$

Now, let us determine the relation between $w_{1\infty}$ and $w_{2\infty}$. Setting the right-hand side of Equation (17) to zero, we obtain $\nu w_{1\infty} - \lambda_2 w_{2\infty} = 0$. Setting the right-hand side of Equation (16) to zero and dividing by $\sqrt{w_{1\infty}^2 + w_{2\infty}^2}$, we obtain $(\lambda_1 w_{1\infty} - \nu w_{2\infty})\sqrt{w_{1\infty}^2 + w_{2\infty}^2} = \|\mathbf{\Sigma}_{xy}\|$.

Recall that the target vector $\boldsymbol{\beta}$ lies in the span of $\{\boldsymbol{v}_1, \boldsymbol{v}_2\}$. Let $\boldsymbol{\beta} = c_1\boldsymbol{v}_1 + c_2\boldsymbol{v}_2$. Since $\mathbf{\Sigma}_{xy} = \mathbf{\Sigma}\boldsymbol{\beta}$, taking the inner product with $\boldsymbol{v}_2$ gives $0 = \boldsymbol{v}_2^\top \mathbf{\Sigma}(c_1\boldsymbol{v}_1 + c_2\boldsymbol{v}_2)$, which yields $\nu c_1 - \lambda_2 c_2 = 0$. Taking the inner product with $\boldsymbol{v}_1$ gives $\|\mathbf{\Sigma}_{xy}\| = \boldsymbol{v}_1^\top \mathbf{\Sigma}(c_1\boldsymbol{v}_1 + c_2\boldsymbol{v}_2)$. Rearranging the terms, we obtain $\lambda_1 c_1 - \nu c_2 = \|\mathbf{\Sigma}_{xy}\|$.

Notice that both $(w_{1\infty}, w_{2\infty})$ and (c_1, c_2) satisfy the same linear equation $\nu x_1 - \lambda_2 x_2 = 0$. This implies they are proportional, meaning there exists a scalar k such that $(w_{1\infty}, w_{2\infty}) = k(c_1, c_2)$. Substituting this into the second equilibrium equation yields $k|k|(\lambda_1 c_1 - \nu c_2)\sqrt{c_1^2 + c_2^2} = \|\Sigma_{xy}\|$. Using $\lambda_1 c_1 - \nu c_2 = \|\boldsymbol{\Sigma}_{xy}\|$ and the fact that $c_1^2 + c_2^2 = 1$ (since $\boldsymbol{v}_1$ and $\boldsymbol{v}_2$ are orthonormal and $\|\boldsymbol{\beta}\| = 1$), this simplifies to $k|k|\|\boldsymbol{\Sigma}_{xy}\| = \|\boldsymbol{\Sigma}_{xy}\|$. Thus, $k = 1$, which proves $(w_{1\infty}, w_{2\infty}) = (c_1, c_2)$. Consequently, we establish that

$$w_{1\infty}^2 + w_{2\infty}^2 = c_1^2 + c_2^2 = 1. \tag{C.31}$$

Using $w_{2\infty} = \nu w_{1\infty}/\lambda_2$, we obtain

$$w_{1\infty}^2 \left(1 + \left(\frac{\nu}{\lambda_2}\right)^2\right) = 1. \tag{C.32}$$

Therefore,

$$\begin{aligned} t - t_1 &= \tau \int_{w_2(t_1)}^{w_2(t)} \frac{dw_2}{(w_1^2 + w_2^2)(\nu w_1 - \lambda_2 w_2)} \\ &\leq \tau \int_{w_2(t_1)}^{w_2(t)} \frac{dw_2}{(w_{1\infty}^2 + w_2^2)(\nu w_{1\infty} - \lambda_2 w_2)} \\ &= \tau \frac{1}{\lambda_2 w_{1\infty}^2 \left(1 + \left(\frac{\nu}{\lambda_2}\right)^2\right)} \int_{w_2(t_1)}^{w_2(t)} \left(\frac{w_2 + \frac{\nu}{\lambda_2} w_{1\infty}}{w_2^2 + w_{1\infty}^2} - \frac{1}{w_2 - \frac{\nu}{\lambda_2} w_{1\infty}}\right) dw_2 \\ &= \frac{\tau}{\lambda_2} \left[\frac{\nu}{\lambda_2} \arctan\left(\frac{w_2}{w_{1\infty}}\right) + \frac{1}{2}\log(w_2^2 + w_{1\infty}^2) - \log\left|w_2 - \frac{\nu}{\lambda_2} w_{1\infty}\right|\right]_{w_2(t_1)}^{w_2(t)}. \end{aligned} \tag{C.33}$$

Let us evaluate the integral using the antiderivative $G(w_2)$:

$$G(w_2) := \frac{\nu}{\lambda_2} \arctan\left(\frac{w_2}{w_{1\infty}}\right) + \frac{1}{2}\log(w_2^2 + w_{1\infty}^2) - \log(w_{2\infty} - w_2). \tag{C.34}$$

Since the integrand is strictly positive for $w_2 \in [0, w_{2\infty})$, $G(w_2)$ is a strictly increasing function. Therefore, for any fixed $\varepsilon > 0$, we have $G(\varepsilon) > G(0)$. Thus,

$$t_2 - t_1 \leq \frac{\tau}{\lambda_2}(G(w_2(t_2)) - G(\varepsilon)) < \tau \frac{1}{\lambda_2}(G(w_2(t_2)) - G(0)). \tag{C.35}$$

Evaluating $G(w_2)$ at the upper bound $w_2(t_2) = (1 - e^{-\delta})w_{2\infty}$ yields:

$$G(w_2(t_2)) = \frac{\nu}{\lambda_2} \arctan\left(\frac{(1 - e^{-\delta})w_{2\infty}}{w_{1\infty}}\right) + \frac{1}{2}\log((1 - e^{-\delta})^2 w_{2\infty}^2 + w_{1\infty}^2) - \log(w_{2\infty} - (1 - e^{-\delta})w_{2\infty}). \tag{C.36}$$

Evaluating $G(w_2)$ at 0, we get

$$G(0) = \frac{1}{2}\log(w_{1\infty}^2) - \log(w_{2\infty}). \tag{C.37}$$

Subtracting $G(0)$ from $G(w_2(t_2))$, we obtain

$$G(w_2(t_2)) - G(0) = \frac{\nu}{\lambda_2} \arctan\left(\frac{\nu}{\lambda_2}(1 - e^{-\delta})\right) + \frac{1}{2}\log\left(\frac{w_{1\infty}^2 + w_{2\infty}^2(1 - e^{-\delta})^2}{w_{1\infty}^2}\right) + \delta. \tag{C.38}$$

Using the fixed-point relation $w_{2\infty}/w_{1\infty} = \nu/\lambda_2$, we can obtain the bound in Inequality (23):

$$t_2 - t_1 \leq \frac{\tau}{\lambda_2}\left[\frac{\nu}{\lambda_2} \arctan\left(\frac{\nu}{\lambda_2}(1 - e^{-\delta})\right) + \frac{1}{2}\log\left(1 + \left(\frac{\nu}{\lambda_2}(1 - e^{-\delta})\right)^2\right) + \delta\right]. \tag{C.39}$$

□

D Derivation of the Generalization Error

Proof of Theorem 4.1. For $\boldsymbol{\Sigma} = \sigma^2(\boldsymbol{I} + \rho\boldsymbol{\mu}\boldsymbol{\mu}^\top)$, the eigenvalues are

$$\lambda_1 = \sigma^2(1+\rho), \quad \lambda_i = \sigma^2 \quad (i = 2, \dots, d). \tag{D.1}$$

Substituting this spectrum into Equation (28) gives

$$\begin{aligned} 1 &= \frac{\lambda}{\kappa(\lambda)} + \frac{1}{n}\sum_{i=1}^{d} \frac{\lambda_i}{\kappa(\lambda) + \lambda_i} \\ &= \frac{\lambda}{\kappa(\lambda)} + \frac{d}{n}\frac{1}{d}\sum_{i=1}^{d} \frac{\lambda_i}{\kappa(\lambda) + \lambda_i} \\ &= \frac{\lambda}{\kappa(\lambda)} + \frac{d}{n}\left(\frac{d-1}{d}\frac{\sigma^2}{\kappa(\lambda)+\sigma^2} + \frac{1}{d}\frac{\sigma^2(1+\rho)}{\kappa(\lambda)+\sigma^2(1+\rho)}\right) \end{aligned} \tag{D.2}$$

In the high-dimensional limit $n, d \to \infty$ with $d/n \to \gamma$, the spike term is weighted by $1/d$ and therefore vanishes. Hence,

$$\begin{aligned} 1 &= \frac{\lambda}{\kappa(\lambda)} + \gamma\frac{\sigma^2}{\kappa(\lambda)+\sigma^2} \\ &= \frac{(\kappa(\lambda)+\sigma^2)\lambda + \gamma\sigma^2\kappa(\lambda)}{\kappa(\lambda)(\kappa(\lambda)+\sigma^2)}. \end{aligned} \tag{D.3}$$

Rearranging the terms, we obtain the quadratic equation:

$$\kappa(\lambda)^2 - (\lambda + (\gamma-1)\sigma^2)\kappa(\lambda) - \sigma^2\lambda = 0. \tag{D.4}$$

Define $\kappa_0 := \lim_{\lambda\to 0^+}\kappa(\lambda)$. Taking $\lambda \to 0^+$ in Equation (D.4) gives

$$\kappa_0^2 - (\gamma-1)\sigma^2\kappa_0 = 0. \tag{D.5}$$

Since $\gamma > 1$ and $\kappa_0 > 0$, we obtain:

$$\kappa_0 = \sigma^2(\gamma - 1). \tag{D.6}$$

Next, differentiate Equation (D.4) with respect to λ:

$$2\kappa(\lambda)\frac{d\kappa(\lambda)}{d\lambda} - \kappa(\lambda) - (\gamma-1)\sigma^2\frac{d\kappa(\lambda)}{d\lambda} - \sigma^2 = 0. \tag{D.7}$$

Therefore,

$$\frac{d\kappa(\lambda)}{d\lambda} = \frac{\kappa(\lambda)+\sigma^2}{2\kappa(\lambda) - \sigma^2(\gamma-1)}. \tag{D.8}$$

Taking the limit $\lambda \to 0^+$, we obtain

$$\lim_{\lambda\to 0^+}\frac{d\kappa(\lambda)}{d\lambda} = \frac{\kappa_0+\sigma^2}{2\kappa_0 - \sigma^2(\gamma-1)} = \frac{\gamma}{\gamma-1}. \tag{D.9}$$

Finally, since $A = \boldsymbol{\mu}^\top\boldsymbol{\beta}$, we decompose $\boldsymbol{\beta}$ as follows.

If $0 \le A < 1$, then

$$\boldsymbol{\beta} = A\boldsymbol{\mu} + \sqrt{1-A^2}\boldsymbol{u}_2, \tag{D.10}$$

where

$$\boldsymbol{u}_2 = \frac{(\boldsymbol{I} - \boldsymbol{\mu}\boldsymbol{\mu}^\top)\boldsymbol{\beta}}{\|(\boldsymbol{I} - \boldsymbol{\mu}\boldsymbol{\mu}^\top)\boldsymbol{\beta}\|} \tag{D.11}$$

is a unit vector orthogonal to $\boldsymbol{\mu}$.

If $A = 1$, then $\boldsymbol{\beta} = \boldsymbol{\mu}$. In this case, let $\boldsymbol{u}_2$ be any unit vector orthogonal to $\boldsymbol{\mu}$.

Therefore, with $\boldsymbol{u}_1 = \boldsymbol{\mu}$,

$$(\boldsymbol{\beta}^\top \boldsymbol{u}_1)^2 = A^2, \quad (\boldsymbol{\beta}^\top \boldsymbol{u}_2)^2 = 1 - A^2, \quad \lambda_1 = \sigma^2(1+\rho), \quad \lambda_2 = \sigma^2. \tag{D.12}$$

Taking $\lambda \to 0^+$ in Equation (27) and using Equations (D.6), (D.9) and (D.12), we obtain

$$\begin{aligned}
\hat{R}_0 =& \lim_{\lambda \to 0^+} \hat{R}_\lambda \\
&= \frac{\gamma}{\gamma - 1} \cdot (\sigma^2(\gamma-1))^2 \cdot \left(\frac{\sigma^2(1+\rho)}{(\sigma^2(\gamma-1) + \sigma^2(1+\rho))^2} A^2 + \frac{\sigma^2}{(\sigma^2(\gamma-1)+\sigma^2)^2}(1-A^2) \right) \\
&= \sigma^2 \gamma(\gamma-1) \left(\frac{1+\rho}{(\gamma+\rho)^2} A^2 + \frac{1}{\gamma^2}(1-A^2) \right) \\
&= \sigma^2 \left(1 - \frac{1}{\gamma}\right) \left(\frac{1+\rho}{(1+\rho/\gamma)^2} A^2 + (1-A^2) \right) \\
&= \sigma^2 \left(1 - \frac{1}{\gamma}\right) \left[1 - A^2 \left(1 - \frac{1+\rho}{(1+\rho/\gamma)^2} \right) \right].
\end{aligned} \tag{D.13}$$

□